Published in "Journal of Comparative Neurology 521(14): 3133–3153, 2013"
which should be cited to refer to this work.

Efferent Connections of the Parvalbumin-Positive (PV1) Nucleus in the Lateral Hypothalamus of Rodents

Marco R. Celio,[1,2]* Alexandre Babalian,[1] Quan Hue Ha,[2] Simone Eichenberger,[1] Laurence Clément,[1] Christiane Marti,[1] and Clifford B. Saper[2]

[1]Anatomy Unit, Department of Medicine and Program in Neuroscience, University of Fribourg, CH-1700, Fribourg, Switzerland
[2]Department of Neurology and Program in Neuroscience, Harvard Medical School, Beth Israel Deaconess Medical Center, Boston, Massachusetts 02215

ABSTRACT

A solitary cluster of parvalbumin-positive neurons – the PV1 nucleus – has been observed in the lateral hypothalamus of rodents. In the present study, we mapped the efferent connections of the PV1 nucleus using nonspecific antero- and retrograde tracers in rats, and chemoselective, Cre-dependent viral constructs in parvalbumin-Cre mice. In both species, the PV1 nucleus was found to project mainly to the periaqueductal grey matter (PAG), predominantly ipsilaterally. Indirectly in rats and directly in mice, a discrete, longitudinally oriented cylindrical column of terminal fields (PV1-CTF) was identified ventrolateral to the aqueduct on the edge of the PAG. The PV1-CTF is particularly dense in the rostral portion, which is located in the supraoculomotor nucleus (Su3). It is spatially interrupted over a short stretch at the level of the trochlear nucleus and abuts caudally on a second parvalbumin-positive (PV2) nucleus. The rostral and the caudal portions of the PV1-CTF consist of axonal endings, which stem from neurons scattered throughout the PV1 nucleus. Topographically, the longitudinal orientation of the PV1-CTF accords with that of the likewise longitudinally oriented functional modules of the PAG, but overlaps none of them. Minor terminal fields were identified in a crescentic column of the lateral PAG, as well as in the Edinger–Westphal, the lateral habenular, and the laterodorsal tegmental nuclei. So far, no obvious functions have been attributed to this small, circumscribed column ventrolateral to the aqueduct, the prime target of the PV1 nucleus. J. Comp. Neurol. 521:3133–3153, 2013.

INDEXING TERMS: axonal tracing; Cre-dependent viral constructs; periaqueductal gray; ventrolateral column; Su3; PV2; blood pressure; vocalization; REM sleep; adeno-associated virus

The lateral hypothalamic area (LHA) is a complex region consisting of many different cell types mingling with the longitudinally directed fibers of the medial forebrain bundle (mfb). In early studies, the projections of the LHA could not be distinguished from those of axons traveling in the medial forebrain bundle by using degenerative techniques (Guillery, 1957; Chi and Flynn, 1971). However, with the advent in the 1970s of more sophisticated, axonal transport-tracing techniques, the anterior, tuberal, and posterior regions of the LHA were found to have different patterns of projection (Saper et al., 1976, 1979; Berk and Finkelstein, 1982). More recently, the projections of much smaller regions of the

Additional Supporting Information may be found in the online version of this article.

This article is dedicated to Antonia Milroy, superb technician, dedicated teacher, and enthusiastic neuroscientist.

Dr. Celio spent sabbatical leaves at Harvard Medical School in 1997 and 2008.

Grant sponsor: the Canton of Fribourg; Grant sponsor: the Swiss National Science Foundation; Grant number: 3100A0–113524; Grant sponsor: the Novartis Foundation; Grant sponsor: the U.S. Public Health Service; Grant numbers: NS33987 and NS072337.

*Correspondence to: Marco R. Celio, Anatomy Unit and Program in Neuroscience, Department of Medicine, University of Fribourg, Rte. A. Gockel 1, CH-1700 Fribourg, Switzerland. E-mail: marco.celio@unifr.ch.

LHA, such as the juxtadorsomedial, juxtaparaventricular, and suprafornical regions, have been examined by using *Phaseolus vulgaris* leucoagglutinin (PHA-L) as an anterograde tracer and cholera toxin B (CTB) as a retrograde tracer (Hahn and Swanson, 2010, 2012). However, these pathways include axons stemming from many chemically and physiologically distinct neuronal populations, which makes it difficult to elucidate their potential functional significance.

The identification of neuropeptides that are specific to the LHA has permitted a much more precise delineation of the connections of the nerve cells that synthesize them. For example, the projections of the orexin- (or hypocretin) secreting neurons and the neighboring melanin-concentrating hormone–secreting neurons can be readily traced, as these peptides are synthesized by cells occurring exclusively in the LHA. Consequently, their projections can be revealed immunohistochemically

Abbreviations

3	Oculomotor nucleus
4	Trochlear nucleus
AAV	Adeno-associated virus
AcbC	Accumbens nucleus, core
AHiAL	Amygdalohippocampal area, anterolateral part
AHiPM	Amygdalohippocampal area, posteromedial part
AID	Agranular insular cortex, dorsal part
AIV	Agranular insular cortex, ventral part
AVPO	Anteroventral preoptic nucleus
aq	aqueduct
B	Basal nucleus of Meynert
Barr	Barrington's nucleus
BDA	Biotinylated dextran amine
BST	Bed nucleus of the stria terminalis
BSTL	Bed nucleus of the stria terminalis, lateral division
BSTMA	Bed nucleus of the stria terminalis, medial division, anterior part
BSTMPI	Bed nucleus of the stria terminalis, medial division, posterointermediate part
BSTMPL	Bed nucleus of the stria terminalis, medial division, posterolateral part
BSTV	Bed nucleus of the stria terminalis, ventral division
Ce	Central amygdaloid nucleus
CG	Central (periaqueductal) gray
CG (med)	Central gray, medial part
CGA	Central gray, alpha part
CLi	Caudal linear nucleus of the raphe
DK	Nucleus of Darkschewitz
DMTg	Dorsomedial tegmental area
DP	Dorsal peduncular cortex
DR	Dorsal raphe nucleus
DRV	Dorsal raphe nucleus, ventral part
DTT	Dorsal taenia tecta
EGFP	Enhanced green fluorescent protein
EW	Edinger–Westphal nucleus
F	fornix
FG	Fluoro-Gold
HDB	Nucleus of the horizontal limb of the diagonal band
HRP	Horseradish peroxidase
IG	Indusium griseum
IL	Infralimbic cortex
IPC	Interpeduncular nucleus, caudal subnucleus
IPR	Interpeduncular nucleus, rostral subnucleus
KF	Kölliker–Fuse nucleus
LC	Locus coeruleus
LDTg	Laterodorsal tegmental nucleus
LH	Lateral hypothalamic area
LHb	Lateral habenular nucleus
LHbM	Lateral habenular nucleus, medial part
LM	Lateral mammillary nucleus
LPAG	Lateral periaqueductal gray
LPB	Lateral parabrachial nucleus
LPBC	Lateral parabrachial nucleus, superior part
LPBE	Lateral parabrachial nucleus, external part
LPBS	Lateral parabrachial nucleus, central part
LPO	Lateral preoptic area
LS	Lateral septal nucleus
LSD and LSV	Lateral septal nucleus, dorsal and ventral part
LSI	Lateral septal nucleus, intermediate part
me5	Mesencephalic fifth nerve
mfb	Medial forebrain bundle
mlf	Medial longitudinal fascicle
mn5	Motor nucleus of trigeminal nerve
MdD	Medullary reticular nucleus, dorsal part
MGP	Medial globus pallidus
mHy	medial Hypothalamus
MiTg	Microcellular tegmental nucleus
MnPO	Median preoptic nucleus
MO	Medial orbital cortex
MPA	Medial preoptic area
MPB	Medial parabrachial nucleus
mt	Mammillothalamic tract
NRTh	Reticular thalamic nucleus
O	Nucleus O
ot	Optic tract
PAG	Periaqueductal gray
Parav. Nu.	Paraventricular nucleus
PB	Parabrachial nucleus
PBP	Parabrachial pigmented nucleus
PC	Paracentral thalamic nucleus
PCRt	Parvicellular reticular nucleus
PDTg	Posterodorsal tegmental nucleus
PFA	Paraformaldehyde
PH	Posterior hypothalamic area
PHA-L	*Phaseolus vulgaris* leucoagglutinin
PN	Paranigral nucleus
PnV	Pontine reticular nucleus, ventral part
PPTg	Pedunculopontine tegmental nucleus
PrL	Prelimbic cortex
PV	Parvalbumin
PV1	Parvalbumin-positive nucleus of the lateral hypothalamus
PV1-CTF	Cylinder of PV1-terminal fields ventrolateral to the aqueduct
PV2	Parvalbumin-positive nucleus ventral of the metencephalic aqueduct
PVA	Paraventricular thalamic nucleus, anterior part
PVP	Paraventricular thalamic nucleus, posterior part
rf	Fasciculus retroflexus
RMC	Red nucleus, magnocellular
RpN	Raphe pontis nucleus
RRF	Retrorubral field
Rth	Reticular thalamic nucleus
RtTgP	Reticulotegmental nucleus of the pons, pericentral part
RVRG	Rostral ventral respiratory group
SC	Superior colliculus
SFO	Subfornical organ
SHi	Septohippocampal nucleus
SI	Substantia innominata
SNR	Substantia nigra, reticular part
SOL	Nucleus of solitary tract
SolM	Nucleus of the solitary tract, medial part
SolVL	Nucleus of solitary tract, ventrolateral part
SPTg	Subpeduncular tegmental nucleus
STh	Subthalamic nucleus
Su3	Supraoculomotor central gray
SubCV	Subcoeruleus nucleus, ventral part
SuM	Supramammillary nucleus
SuML	Supramammillary nucleus, lateral part
VDB	Nucleus of the vertical limb of the diagonal band
vlPAG	Ventrolateral PAG
VTA	Ventral tegmental area
VP	Ventral pallidum
VTT	Ventral taenia tecta
WGA	Wheat germ agglutinin
ZI	Zona incerta

(Bittencourt et al., 1992; Peyron et al., 1998; Chemelli et al., 1999). Although these studies have furnished useful information regarding the possible functions of the implicated cell groups, the methodology is of course applicable only to those neuronal populations of the LHA that contain unique peptides.

A more common situation is exemplified by the parvalbumin-positive (PV1) nucleus (Celio, 1990; Girard et al., 2011; Meszar et al., 2012), which is lodged in the LHA, adjacent to the optic tract. Although the group of PV-positive neurons in this location is quite distinct, many other PV-immunoreactive neurons are scattered throughout the brain. Consequently, the projections of the PV1 nucleus cannot be inferred simply by following the ramifications of PV-immunoreactive axons. To characterize the projections of the PV1 nucleus in the present study, nonselective anterograde and retrograde tracing methods were utilized in rats, and chemoselective tracing techniques in PV-Cre mice (Hippenmeyer et al., 2005). In the latter approach, adeno-associated viral (AAV) vectors expressing red or green fluorescent proteins in a Cre-dependent manner (Yonehara et al., 2011) were injected into the PV1 nucleus of PV-Cre mice. These experiments in rodents permitted us to identify a narrow column located at the edge of the periaqueductal gray (PAG), ventrolateral to the aqueduct, as the prime projection target of the PV1 nucleus.

MATERIALS AND METHODS

The overall study was approved by the Veterinary Commission for Animal Research of the Canton of Fribourg, Switzerland. All animals prepared for this study were housed in state-of-the art animal facilities according to the strict Swiss animal experimentation law. Other animals, drawn from previously published studies (Herbert et al., 1990; Moga et al., 1990; Hurley et al., 1991), had been housed at the University of Chicago Pritzker School of Medicine animal facility, and protocols had been approved by that institution's animal care and use committee.

Rat tracing experiments

Wistar rats of both sexes, weighing 275–300 g, were used for the current study. A substantial body of the data presented is drawn from the retrospective analysis of archival specimens that had been prepared for previously published studies (Herbert et al., 1990; Moga et al., 1990; Hurley et al., 1991). The methods used in those experiments were described in detail in those publications, and involved anterograde and retrograde tracing with wheat germ agglutinin–horseradish peroxidase (WGA-HRP), revealed by a tetramethylbenzidine method, and anterograde tracing with PHA-L, demonstrated immunohistochemically.

Antero- and retrograde tracing

The animals prepared for the current study were deeply anesthetized with a mixture of Ketalar (Parke-Davis, Ann Arbor, MI; 75 mg/kg of body weight) and xylazine (Streuli, Uznach, Switzerland; 10 mg/kg of body weight) prior to tracer application and perfusion. By using a Kopf (Tujinga, CA) stereotactic apparatus, the brains of six rats were bilaterally injected in the region of the PV1 nucleus of the lateral hypothalamus with 20 nl of biotinylated dextran amine at the following coordinates: anteroposterior Bregma −2.56 mm; dorsoventral −8.6 mm; lateral +2.4 mm and −2.4 mm. After 2 weeks, rats were perfused with 0.9% NaCl, followed by 4% paraformaldehyde (in 0.1 M phosphate buffer, pH 7.3; PFA). The brains were excised and cryoprotected overnight with 18% sucrose. Coronal, 40-µm-thick cryostat sections were prepared from the chemically fixed brains, and incubated for 24–48 hours at 4°C with a monoclonal antibody against parvalbumin (PV 235, Swant, Marly, Switzerland) diluted 1:10,000 in 0.2% Triton X-100 and 10% horse serum. They were washed in the same buffer and then incubated for 2 hours in the dark with goat anti-mouse IgG/Cy2 (1:200; Jackson ImmunoResearch, West Grove, PA) to stain the primary antibody, and with Streptavidin-Cy3 (1:1'000) (Jackson ImmunoResearch) to detect the biotinylated dextran. After washing, sections at the relevant level were mounted and examined with a Zeiss Axiophot fluorescence microscope.

In three rats for each site, 30–50 nl of a 4% solution of Fluoro-Gold (Fluorochrome, Denver CO) in saline were injected into one of the following regions: PAG (anteroposterior −6.04 mm; mediolateral 0.8 mm; dorsoventral −5.6 mm) and laterodorsal tegmental nucleus (anteroposterior −8.72 mm; mediolateral 0.8 mm; dorsoventral −7 mm). After sectioning, all slices containing the hypothalamus were incubated with the PV235 antibody and further prepared for indirect fluorescence microscopy as described above.

The archival rat material analysed to trace the connections to the PV1 nucleus is listed in Tables 2 and 3. These previous experiments revealed the PV1 nucleus to be targeted with fair precision by some injections of WGA-HRP into the lateral hypothalamus (Moga et al., 1990). Likewise, retrograde tracing experiments from the midbrain have been reported by Hurley et al. (1991) and Herbert and Saper (1992).

Mouse tracing experiments

Expression of the enzyme Cre-recombinase in the PV-positive neurons of the PV1 nucleus of PV-Cre mice

TABLE 1.

Antibodies Used

Antibody	Source	Manufacturer	Details
PV235	Purified carp parvalbumin	Swant	Mouse monoclonal, lot 10–11F
PV28/25	Recombinant rat parvalbumin	Swant	Rabbit polyclonal, lot 5.10
CART	Synthetic peptide (amino acids 55–102)	Phoenix Pharmaceuticals	Rabbit polyclonal, lot 00324

TABLE 2.

Anterograde tracing in rats: Projections of Neurons Located Within or Close to the Rat PV1 Nucleus (Archival Material)[a]

Experiment	Tracer	Injection site	Stained fibers and terminals in:
R93	WGA-HRP	Lateral hypothalamus	DP, IL (lower layers V–VI), *LSI*, *LSD*, and *LSV*, VDB, HDB, MPA, BSTV, BSTVI, BSTMA, AVPO, LPO, BSTL, BSTMPL, BSTMPI, AHiAL, LHBM (bilateral), AHiPM, SuM, IPR, **PAG** (mid), PN,VTA, SNR, IPC, RRF, **PAG**, Cli, **Su3**, PPTg, DR, **PAG**, LPBS, LPBC, LPBE, MPB, LPB, **LDTg**, Rpn, Barr, DMTg, CGA, O, LC, between LC and PDTg, SolM, SOL
R 189	WGA-HRP	Lateral hypothalamus	*LSI*, HDB, CLi, DP (or IL), **LPAG**, PPTg, PB (some), **LDTg**, Barr (few), LC, PDTg
R 451	*Phaseolus vulgaris* agglutinin (PHA)	Lateral hypothalamus	AID, AIV, DP, DTT, SHi, IL, AcbC, IG, *LSD*, HDB, VP, BST, Parav. Nu., PVA, PVP, B, SI, *Ce*, *LHb*, PH, **LPAG**, **EW**, **Su3**, 3, VTA, RRF, RtTgP, Pptg, Sptg, **LDTg**, Barr-region, *LPB*, *MPB*, SubCV, PnV, PCRt, SolVL, MdD, Sol
R 877	PHA-L	Tuber cinereum	Prl, MO, IL (lower layers V–VI), DP, DTT, Shi, VDB, LHb (terminals), *Ce*, **PAG**, LH, SuML, PBPPP, DLPA, GRLi, VTA, MiTg, PB, KFCGA, RVRG
R 878	PHA-L	Supraoptic nucleus (+ most anterior part of PV1)	Prl, IL, MO, VTT, IL, DP, AIV, AID, VDB, LS, MnPO, SFO, LHbM, DRV, PB, **LDTg**, RVGR

[a]The regions indicated in bold typeface are those that have been shown in the present study to be targeted by the PV1 nucleus. The regions in italics are those that have been demonstrated to have no connections with the PV1 nucleus. The regions written in standard fonts are probably targets of lateral hypothalamic neurons unrelated to the PV1 nucleus. The terminal fields observed in experiments R93, R189, and R451, are depicted in Figure 2B. For abbreviations, see list.

was demonstrated by breeding 129P2-Pvalb<tm1(***cre***)Arbr>/J mice (Hippenmeyer et al., 2005) with B6;C3-Tg(CAG-DsRed,-EGFP)5Gae/J mice (Jackson Laboratory, Bar Harbor, ME). In the resulting mice, only PV neurons expressing CRE-recombinase synthesize green fluorescent protein, whereas all other neurons remain red. In these mice, all of the PV-positive neurons in the PV1 nucleus were enhanced green fluorescent protein (EGFP)-positive, and all of the EGFP-positive neurons in the PV1 were PV-immunoreactive. Furthermore, PV immunostaining was routinely performed to detect the coexistence of this calcium-binding protein with the viral or the retrograde (e.g., Fluoro-Gold) tracers.

To study the projections of the PV1 cell group in mice (25–35 g body weight), the brains of PV-Cre mice (129P2-Pvalb<tm1(***cre***)Arbr>/J) (Hippenmeyer et al., 2005) were stereotactically injected with a volume of 20–60 nl on the left side (or bilaterally) at coordinates: anteroposterior Bregma −1.5 mm, mediolateral 1.3 mm, and dorsoventral 4.9–5.1 mm with the following Cre-dependent viral construct (Yonehara et al., 2011):

- Serotype 7 AAV EF1a-DIO-ChR2-mCherry-WPRE

In a few cases (see Table 4), the following Cre-dependent constructs were used:

- Serotype 7 AAV EF1a-DIO-ChR2c-2A-DsRed2-WPRE (e.g., 218/11 dx)
- AAV2/1.CAG.FLEX.EGFP.WPRE.bGH (e.g. 502/12)
- AAV2/9.CAG.FLEX.EGFP.WPRE.bGH (e.g. 503/12)

In the first construct, the mCherry was a fusion protein with channelrhodopsin, resulting in the red fluorescence being targeted to the outer membranes of the transfected cells. In the second construct, the 2A linker segment was post-translationally deleted, producing DsRed2 protein that was localized to the cytoplasm of transfected neurons. The third and fourth constructs led to the strong expression of EGFP in Cre-positive cells. They were developed by the Allen Institute and are available commercially from the Vector core at the University of Pennsylvania (http://www.med.upenn.edu/gtp/vectorcore/). Retrograde fluorogold tracing

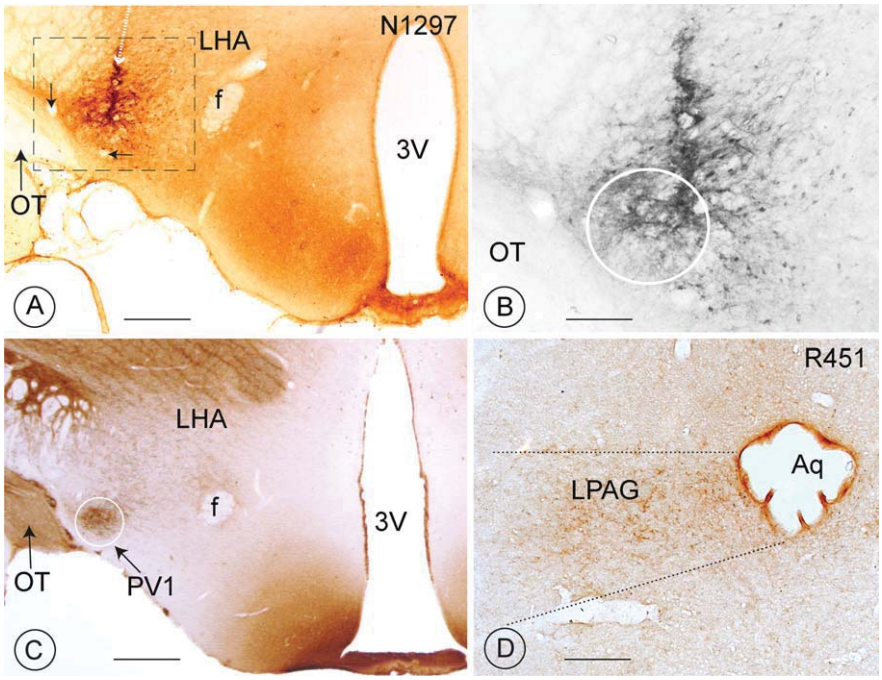

Figure 1. Anterograde tracing from the PV1 nucleus in rats. **A,B:** BDA was used as an anterograde tracer. The tip of the micropipette (represented by the white broken arrow in A) deposited the tracer in a region that includes the PV1 nucleus (white circle in B; injection N 1297). The results of this and of similar experiments were used in the compilation of the Abbreviations list and Table 2. The two small black arrows point to vessels that can also be observed in Figure 5C (white arrows), cut at a similar level in the mouse brain. **C:** Immunohistochemical revelation of PV to indicate the location and size of the PV1 nucleus at a level corresponding to Figure 1A. Note the paucity of other PV-positive elements in the close surroundings of the PV1 nucleus. **D:** Anterograde PHA-L tracing of axon terminals stemming from neurons that were injected in the lateral hypothalamic region, which includes the PV1 nucleus (injection 451; see also Table 2). These axon terminals are widely distributed throughout the cross-sectional area of the lateral PAG. For abbreviations, see list. Scale bar = 0.5 mm in A,C; 0.25 mm in B,D.

experiments were performed similar to those in rats (see above).

Four weeks later, the mice were transcardially perfused with 0.9% NaCl followed by 4% PFA. The brains were excised and processed as described above for rats, with the exception that 80-µm-thick (instead of 40-µm) sections were produced. The sections were then incubated with a rabbit PV antiserum (PV25, Swant, Marly) and then processed for double fluorescence with a biotinylated secondary antibody and Streptavidin-Cy2 or Cy3 (or Alexa 488). The sections were mounted and analyzed under either a fluorescence microscope (Zeiss Axiophot equipped with a Spot-camera (2M sampler), a Leica 6000 epifluorescence microscope equipped with a Hamamatsu C4742-95 camera, a Nanozoomer (Hamamatsu), or a confocal microscope (Leica CTR 6500).

Control tracing experiments

Five control experiments were performed to check whether the projection of PV-immunoreactive structures located along the needle track to the PV1 nucleus (e.g., thalamic reticular nucleus, subthalamic nucleus, zona incerta, medial hypothalamus) contributed endings to the terminal fields in the PAG (see Table 4, experiments 189/11, 415/12, 416/12, 512/12, 513/12). Injections were performed at different mediolateral (1 mm instead of 1.4 mm) and dorsoventral (4.6 mm instead of 5.1 mm) levels.

Characterization of antibodies (Table 1)

Antibodies against parvalbumin (PV235 and PV28/25, all Swant, Marly, Switzerland) recognize only one band of 12 kDa MW in Western blots of brain extract in various species, including rat and mouse. They stain the brain in a pattern consistent with previous results (Celio, 1990) and do not produce staining in the brain of PV knockout mice (Schwaller et al., 1999).

The CART antibody (H-003–62, lot 00324) used to identify the cortically projecting subdivision of the Edinger–Westphal nucleus was acquired from Phoenix Pharmaceuticals (Burlingame, CA). It was produced against synthetic peptides (amino acids 55–102) with no cross-reaction with similar peptides, and its staining

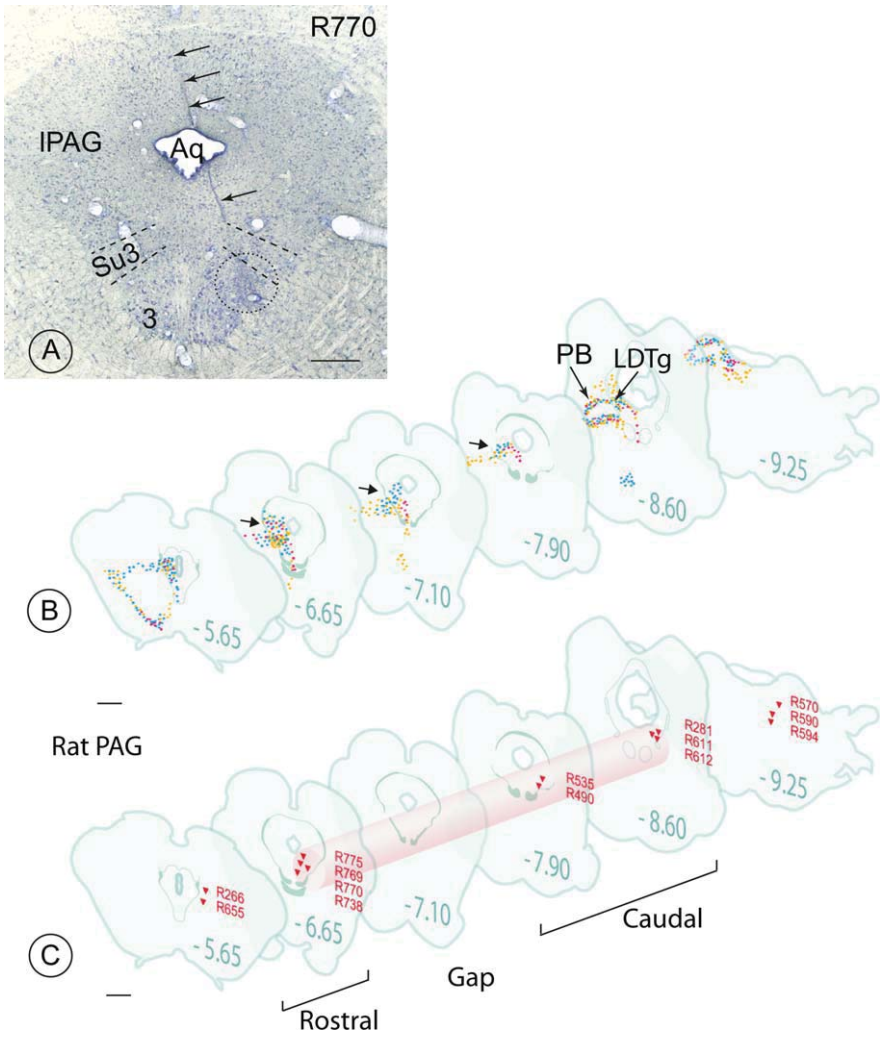

Figure 2. Anterograde tracing from the lateral hypothalamus and retrograde tracing from the rat PAG (archival material). **A:** The track left by the micropipette that deposited the WGA-peroxidase (injection R770, Table 3) ventrolateral to the aqueduct is marked with black arrows. The approximate portion ventrolateral to the aqueduct that was exposed to this retrograde tracer is encircled (stippled circle). Note the proximity of the pipette tip to the Su3 region. **B:** Axon terminals (small colored points) are depicted. Three anterograde tracing experiments are jointly summarized (red, injection R189; yellow, injection R93; and blue, injection R451 (Table 2). Note the similarities between the three specimens in the distribution patterns of the terminals ventrolateral to the aqueduct (short arrows at levels −6.65, −7.10, and −7.90), in the parabrachial nuclei (PB) and the laterodorsal tegmental nucleus (LDTg). However, most of the terminals in the PB apparently do not come from the PV1 cell group. **C:** The location of the needle tip in 14 retrograde tracing experiments is indicated by red triangles. Only nine injections located between level −6.65 and −8.60 succeeded in filling retrogradely neurons in the PV1 (see Table 3, e.g., injection R770, also depicted in Fig. 2A). These injection sites occupy a virtual "column" (light red) located ventrolateral to the aqueduct and composed of a rostral and a caudal part interrupted approximately at level −7.10 by a short gap. Drawing modified from Swanson (2004). For abbreviations, see list. Scale bar = 0.8 mm in A; 1.7 mm in B,C.

was inhibited by adsorption with the immunizing peptide (1 μg/μl). The staining pattern was consistent with previous localization results (Kirouac et al., 2006; Reeber and Sillitoe, 2011).

Photomicrographs

Images were imported in Photoshop (Adobe Systems, San Jose, CA), and contrast, brightness, and sharpness were adapted, if necessary. The image stacks were prepared with ImageJ software, and the figures were mounted with Adobe Illustrator.

RESULTS

Experiments in rats

Tracers that were injected into the ventrolateral part of the hypothalamus always extended beyond the

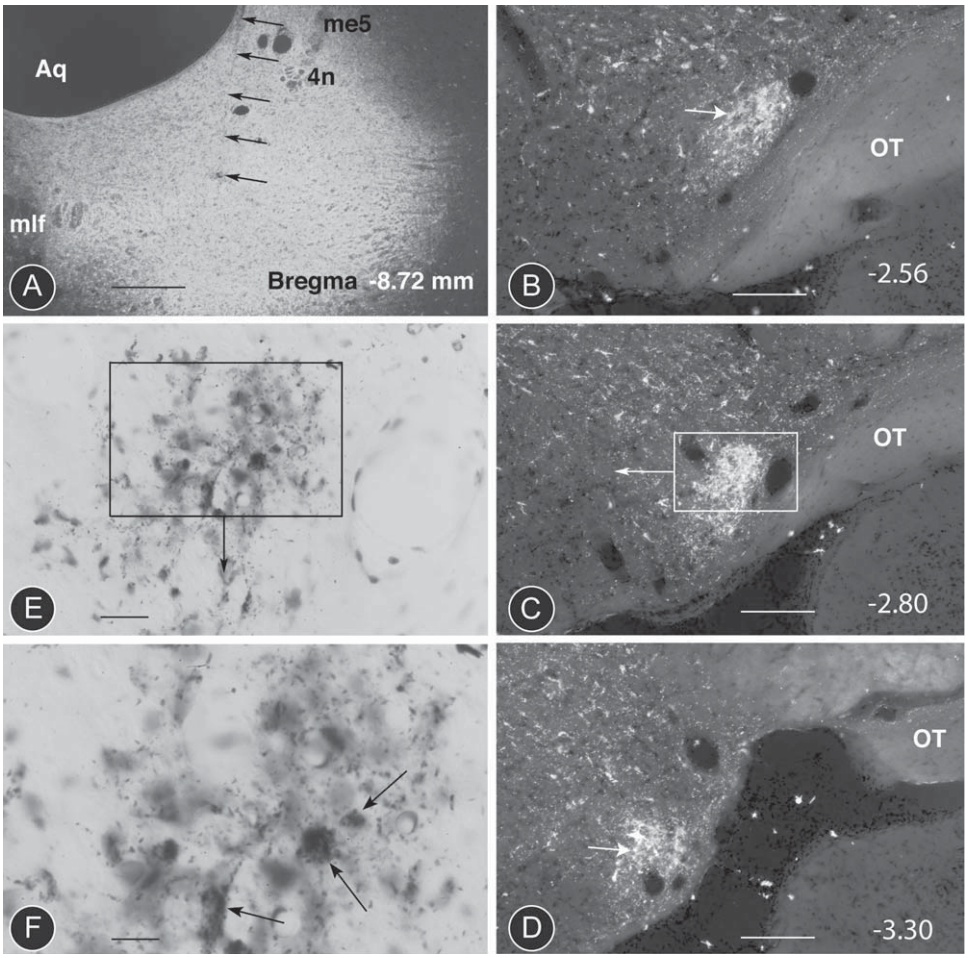

Figure 3. WGA–HRP retrograde tracing from the distal PAG in the rat. **A:** Darkfield image of a WGA–HRP injection into the caudal PAG at level −8.72 according to Paxinos and Watson (1999). The track left by the micropipette is indicated with thin black arrows. The tip of the micropipette is located within the ventrolateral PAG at the level of the LDTg (fifth arrow). Injection 490 (Table 3). **B–D:** Retrograde filling of neurons in the PV1 nucleus of the same animal at three different levels (−2.56, −2.80, and −3.30). In addition to the cells in the PV1 nucleus (arrows), other retrogradely labeled neurons are scattered throughout the lateral hypothalamic area. **E,F:** Brightfield images of the same PV1 nucleus revealing the presence of some retrogradely labeled neurons of different sizes (arrows in F) and considerable axonal labeling (small spots) suggesting a reciprocal projection. Counterstaining with Nissl stain. For abbreviations, see list. Scale bar = 0.25 mm in A; 0.3 mm in B–D; 25 μm in E,F.

borders of the PV1 nucleus (Fig. 1A,B). In the experiments described here, neurons in the PV1 group did indeed take up the anterograde tracer biotinylated dextran (Fig. 1) or WGA-HRP or PHA-L, but other, unrelated nerve cells likewise transported the injected tracer. Hence, the resulting projections include more than would have been expected if only the PV1 neurons had been targeted. A list of the terminal fields recognized in five such experiments is given in Table 2, and a schematic drawing of their localization in the mid- and hindbrain is provided in Figure 2B.

The major targets of the lateral hypothalamus known from the literature, received anterogradely labeled axons, including the infralimbic cortex, the septum, the amygdala, the habenula, the lateral PAG (Figs. 1D, 2B), and the parabrachial nuclei (Fig. 2B). In three rats, terminal fields of labeled axons were also observed in the ventrolateral part of the PAG (highlighted with different colors—red, blue, and green—in Figure 2B).

To determine which of these sites might be specific targets of the PV1 nucleus, their inputs were retrogradely traced. Retrogradely labeled neurons in the PV1 nucleus were seen after injections into only the lateral and the ventrolateral PAG (Figs. 2A,C, 4E) and the laterodorsal tegmental nucleus (Figs. 3, 4B, Table 3) of archival and fresh material.

To determine the topography of the PV1 projection to the rat PAG, we examined retrograde labeling after injections in the lateral or ventrolateral PAG, or in the reticular formation just outside the PAG, in 14 cases

TABLE 3.

Retrograde tracing experiments in Rats: Injections in the PAG (Archival Material)[a]

Experiment	Tracer	Injection site	Labeling in the PV1 nucleus	Localization in PV1	Density
R 266	WGA-HRP	LPAG	None	No neurons; no terminals	-
R 655	WGA-HRP	PAG, Mn5	None	Only terminals	+++
R 281	WGA-HRP	LPAG, LPt	Perikarya and terminals	Neurons throughout	+++
R 490	WGA-HRP	PAG vl (level 6.72)	Perikarya	Neurons middle-caudal part	++
R 535	WGA-HRP	PAG, IVn, IIIPC	Perikarya and terminals	Neurons throughout bilateral	+
R 738	WGA-HRP	PAG, EW, Su3	Perikarya and terminals	Neurons caudal portion	++
R 769	WGA-HRP	PAG	Perikarya	Neurons caudal portion	+++
R 770	WGA-HRP	PAG, Su3	Perikarya	Neurons throughout	+++
R 775	WGA-HRP	PAG, EW, Su3	Perikarya and terminals	Neurons mid-caudal level	+
R 611	WGA-HRP	LDTg	Perikarya and terminals	Neurons + terminals throughout	+++
R 612	WGA-HRP	LDTg	Perikarya and terminals	Neurons + terminals throughout	+
R 570	WGA-HRP	LDTg, Barr	Terminals	Few neurons + terminals caudal	++
R 590	WGA-HRP	Reticular formation ventral to Barr, tip in DMTG at −9.16	Terminals	Terminal throughout	++
R 594	WGA-HRP	Reticular formation ventral to Barr	Terminals and a few perikarya	Terminals throughout	++

[a]Results of archival tracing experiments with WGA-HRP injected in the midbrain. The localization of the injections sites is indicated in Fig. 2C. +, low; ++, high; +++, very high. For Abbreviations, see list.

(the locations of the needle tips are indicated by red triangles in Fig. 2C). The injection of a retrograde tracer close to the PAG in the rostral midbrain (R266 and R655; level −5.65. Fig. 2B) did not lead to filling of the nerve cells in the PV1 nucleus (Table 3). Three injections of a retrograde/anterograde tracer into the pons just ventral to the dorsal tegmental nucleus (R570, R590, and R594; Fig. 2C) revealed only terminal fields (and a few perikarya) in the region occupied by the PV1 nucleus (Table 3). Only the nine injections into the ventrolateral quadrant of the midbrain PAG (Fig. 2C) led to successful retrograde filling of many neurons in the PV1 nucleus (Table 3). Thus, a longitudinal column of successful retrograde injections in the PV1 nucleus was located in the rat ventrolateral PAG, and spanned a length of approximately 2 mm (Fig. 2C; level: −6.65 to −8.60).

As another example, Figure 3A shows the result of a retrograde tracer injection close to the distal ventrolateral PAG and laterodorsal tegmental nucleus. Although other neurons in the lateral hypothalamus were also retrogradely labeled (Fig. 3B–D), the characteristic PV1 group was nevertheless discernible as an intensely labeled cluster (Fig. 3B–D). These findings are summarized in Table 3.

Injections of retrograde tracer in areas such as the lateral septum, the central nucleus of the amygdala, and the parabrachial nuclei, which are known to receive inputs from the lateral hypothalamus, did not lead to labeling of the PV1 nucleus.

Analysis of archival material after retrograde tracing was complemented and confirmed by an evaluation of freshly prepared double-stained specimens: neurons of the lateral hypothalamus that projected to the region of the laterodorsal tegmental region were indeed PV-positive. Figure 4 reveals that when Fluoro-Gold was injected close to the caudal part of the ventrolateral PAG/laterodorsal tegmental nucleus (Fig. 4A,B,E), it was transported back (Fig. 4C,G) to the small PV-positive neurons (Fig. 4D,H) in the PV1 nucleus of the lateral hypothalamus.

Experiments in mice

In the 129P2-Pvalb<tm1(***cre***)Arbr>/J × B6;C3-Tg(CAG-DsRed,-EGFP)5Gae/J mouse, all PV-immunoreactive neurons of the PV1 nucleus expressed EGFP, thus confirming the presence of Cre-recombinase (Fig. 5A,B). Notwithstanding the fact that the PV1 nucleus is near other PV-immunoreactive cell groups, the AAV-mCherry-labeled neurons were almost entirely within the PV1 nucleus (Fig. 5C,D and E–J). The PV1 nucleus was often clearly visible as a compact cluster of cells emitting a red-fluorescent signal in the outermost part of the ventrolateral hypothalamus (Fig. 5C,D). Although not all of the PV-positive neurons of the PV1 nucleus were labeled by the viral construct (Fig. 5D,E-J; see Table 4 for an approximation of the number of infected cells in each experiment), virtually all of the virus-infected neurons were PV-positive. In most cases, small numbers of unrelated PV-positive neurons that lay along the track of the injection needle were labeled (Fig. 6A). These cells were located in the ventrobasal tip of the thalamic reticular nucleus, the medial edge of the

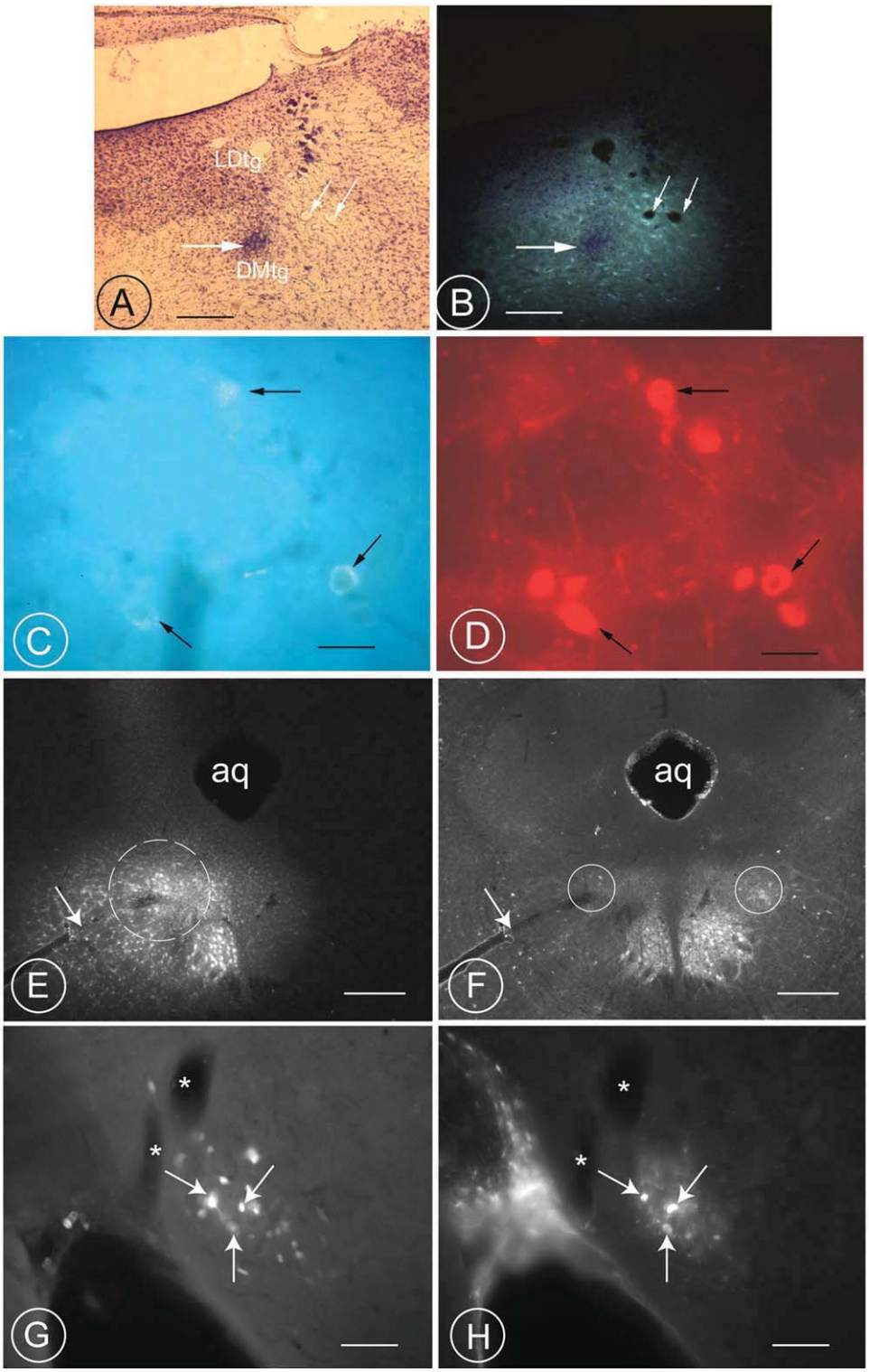

Figure 4. Retrogradely labeled neurons in the rat PV1 nucleus are PV-positive. **A,B:** Fluoro-Gold was injected into the tegmental area at Bregma level −9.16. The thick horizontal arrow in A indicates the location of the needle tip. The same region is depicted in B after illumination with ultraviolet light. Under these illumination conditions, the Fluoro-Gold label is seen to have diffused from the needle tip into the laterodorsal tegmental nucleus. The slender arrows in A and B denote cross sections through two landmark vessels. **C,D:** Three retrogradely labeled neurons (arrows in C) are visible within the ipsilateral PV1 nucleus of the same animal (Bregma level −3.30). In D, the same section, incubated with an antiserum against PV, reveals these three neurons (arrows) to be immunoreactive for this marker protein. **E,F:** Fluoro-Gold applied in the region ventrolateral to the rat PAG (dashed circle in E), including the region characterized by a high concentration of PV-positive terminals (circle in F). The arrow in E and F points to a large vessel passing through the PV-rich region. **G,H:** Retrogradely Fluoro-Gold–filled neurons are concentrated in the region of the PV1 nucleus (G, DAPI filter), and some of them (arrows) express PV immunoractivity (H, Cy3 filter). Both large and small cells are retrogradely filled (G). Note the presence of two large vessels in the vicinity of the PV1 nucleus (asterisks). For abbreviations, see list. A magenta–green version of this image is included as supplementary Figure 1. Scale bar = 0.3 mm in A,B,E,F; 20 μm in C,D; 75 μm in G,H.

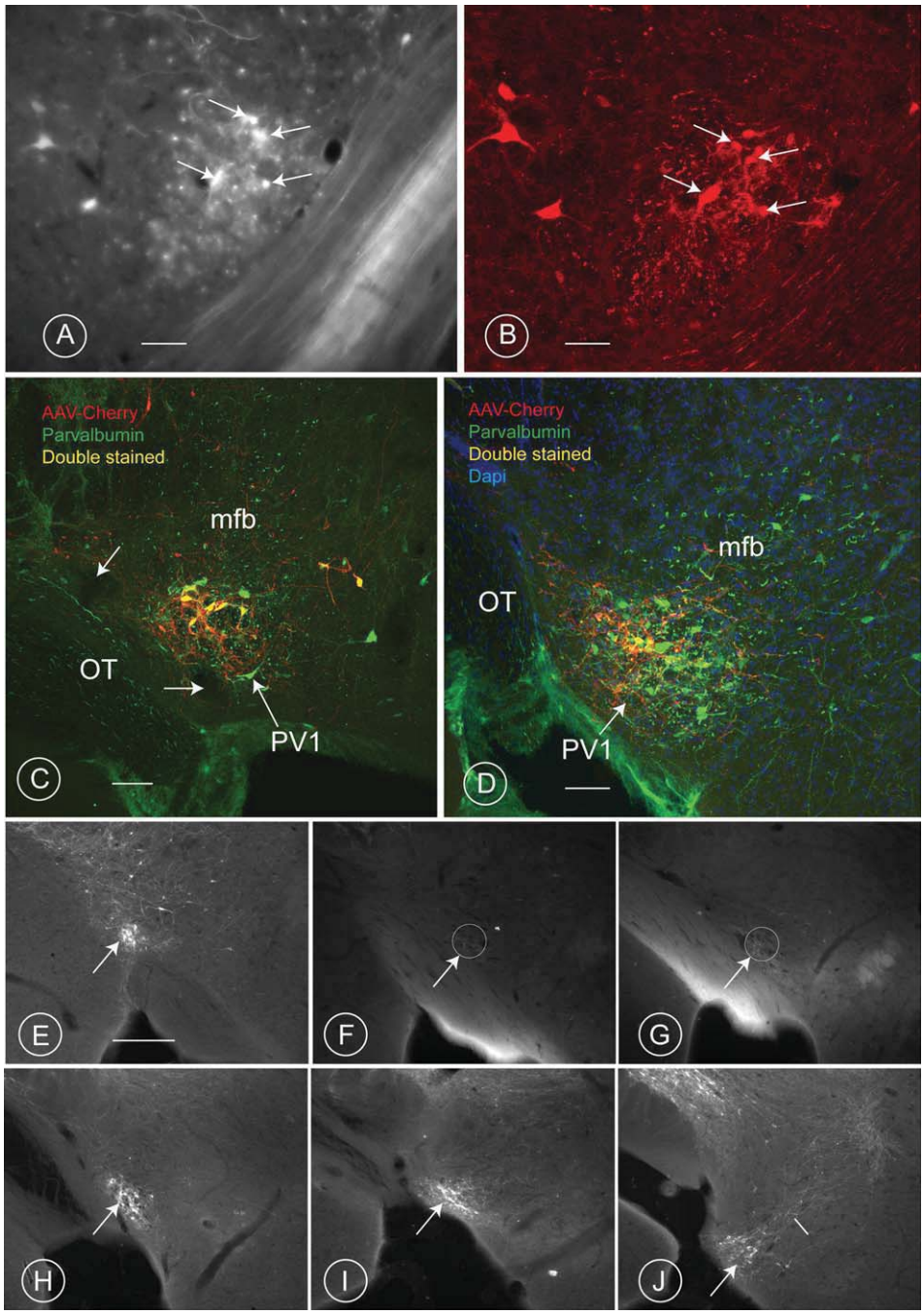

Figure 5. Adeno-associated viral construct injections in the PV1 nucleus of the mouse. **A,B:** Breeding PV-Cre mice with EGFP-floxed mice gave rise to offspring in which all the neurons in the PV1 nucleus are expressing EGFP (A, fluorescent microscopy) and are also PV-positive (B, confocal microscopy). Some double-labeled cells are indicated by white arrows. **C,D:** The Cre-dependent adeno-associated virus-mCherry construct has been taken up by some of the cells (red) in the PV1 nucleus, which are colabeled with a Cy2-tagged antibody against PV (green). Some of the red (mCherry-labeled) neurons are also green PV-positive cells, so the concurrent fluorescence signals appear yellow. However, a few AAV-infected cells emit only a red signal, owing to the poor penetration of the PV antibody through this (80 μm) thick section. The image in C (experiment 218-11), is taken at the posterior level of the PV1 nucleus, and that in D at its caudal extremity. The two white arrows in C indicate vessels that can also be observed in Figure 1B (small black arrows), cut at a similar level in the rat brain. **E–J:** Six consecutive coronal sections at distances of approximately 160 μm from each other through the region of the mouse PV1 nucleus from rostral (E) to caudal (J) (injection 188/11). The AAV-cherry-positive group of neurons in the PV1 is highlighted with an arrow. The intermediate portion of the PV1 nucleus (F,G) remained unlabeled in this experiment. The small white line in J points to streaming axons. A magenta-green version of this image is included as supplementary Figure 2. For abbreviations, see list. Scale bar = 30 μm in A–D; 0.2 mm in E (applies to E–I,J).

TABLE 4.

Experiments in Mice: Cre-Dependent Viral Tracer Injection in the PV1

PV1	Tracer				Distribution in the rostrocaudal axis of the PV1 nucleus					Colabeled structures						Terminals								
Mouse	AAV-Cherry	AAV-Red	AAV-GFP	Inj.	Prox.	Interm.	Post	Dist.	Total infected neurons	NRTh	MGP	STh	Medial Hypoth. neuron	LM	SNR	LHb	rf	PAG EW	PAG Lat	PAG Su3	PAG PV2	dMTG	SC	RMC
188/11	X			PV1	0	27	27	40	94	+	++	+	(+)	n.e.	n.e.	-	-	+	-	+	-	-		
189/11	X			PV1	0	15	8	5	28	+	++	(+)	+	+	++	+	+	+	-	+	+	-	+	+
197/11	X			PV1	20	0	1		21	(+)	+	(+)	(+)	(+)	+	-	-	+	+	+	+	+	+	
198/11	X			NRTh,STh	0	0	0	0	0	+++	+	(+)	-	-	-	-	-	+	+	-	-	-	+	
218/11Sin	X			PV1	2	12	8	23	45	+	++	+	+	+	+	-	+	(+)	-	++	+	(+)	+	
218/11 Dx		X		PV1	1	7	15	4	58	+	(+)	+	+	-	-	-	-	-	-	+	+	-		
237/11	X			PV1	0	16	27	15	26	+	-	++	+	-	-	+	-	++	+	++	+	-		
238/11	X			PV1	2	5	16	7	30	+	++	++	++		+	++	+	-	+	++	+	++		
64/12	X			PV1	20	17	13	13	63	-	++	++	++	++	++	++	+	++	+	++ 640µm	+ 480µm	-	+	+
65/12	X			PV1	9	12	13	2	36	-	+	+	++	-	+	-	-	+	+	++ 560µm	+ 480µm	(+)		
66/12	X			PV1	15	17	7	31	70	-	++	+	++	++	-	-	-	-	+	++ 480µm	+ 480µm	+		
415/12	X			NRTh,STh	0	0	0	0	0	+++	+	++	-	-	-	+	-	-	-	-	-	-	-	
416/12	X			med Hypoth	0	0	0	0	0	-	-	-	++	-	-	-	-	-	-	-	-	-	-	-
502/12			X	PV1	12	10	20	8	50	+	+	+	-	-	-	+	-	-	-	++	++	-	-	
503/12			X	PV1	2	14	8	20	44	+	+	+	-	-	-	+	-	-	-	++	++	-	-	
512/12			X	NRTh,STh	0	0	0	0	0	+++	+	++	-	-	-	+	-	-	-	-	-	-	-	
513/12			X	med Hypoth	0	0	0	0	0	+++	++	+	++	-	-	-	-	-	-	-	-	-	-	
546/12			X	PV1	5	7	12	24	48	+	+	++	-	-	-	+	-	-	-	++	+	-	-	

Results of tracing experiments with various AAV-viral constructs injected in the PV1 nucleus. Abbreviations: (+), faint positive; +, positive ; ++, strongly positive; +++, very strong; -, negative; n.e., not evaluated. For other abbreviations, see list.

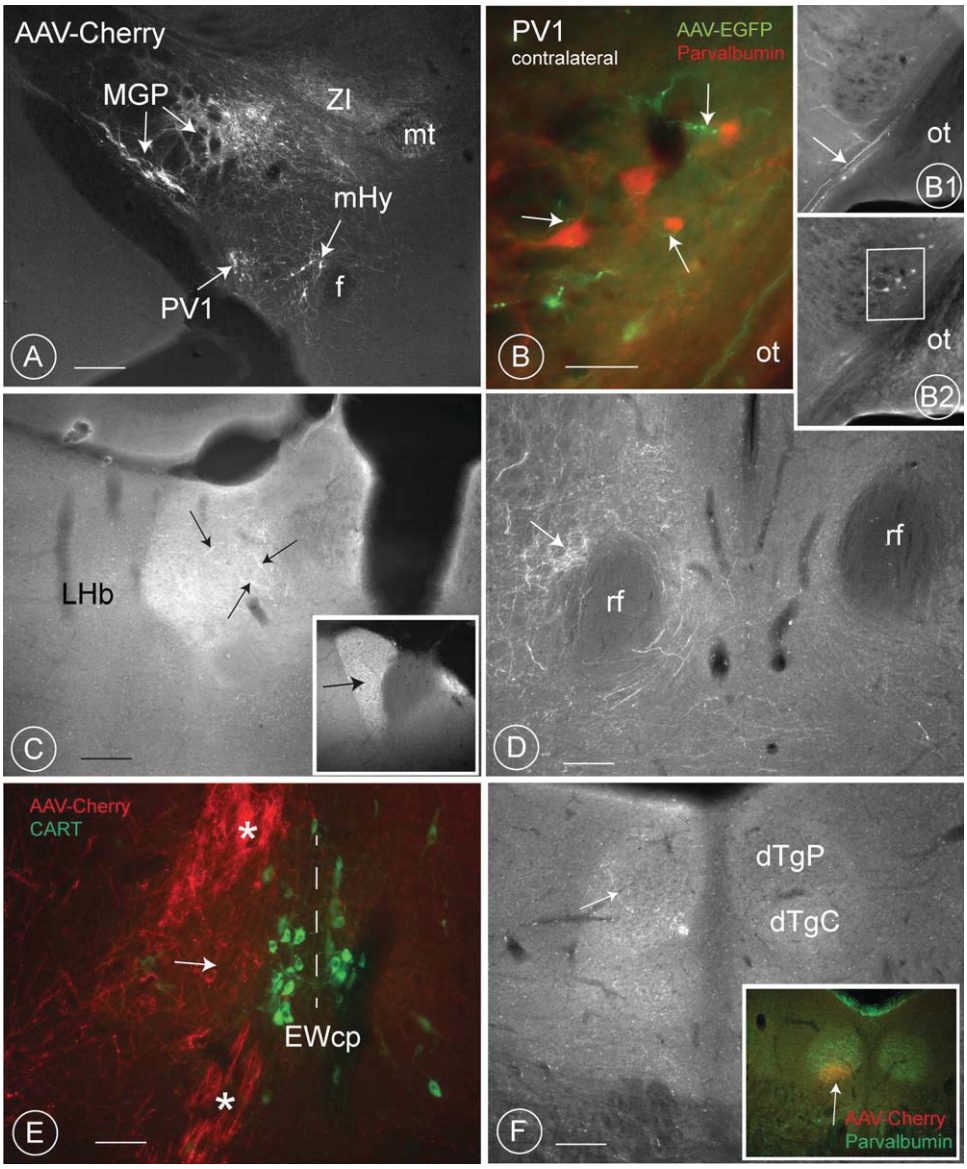

Figure 6. AAV- colabeling of other structures in the mouse diencephalon. **A:** In addition to the PV1 nucleus, neurons in the medial globus pallidus (MGP, also called the entopeduncular nucleus), the subthalamic nucleus, the reticular nucleus of the thalamus (in the picture only axons are visible for these two structures; cell bodies are at another level) and the Zona incerta also took up the viral construct (see Table 4 for details). Injection 64/12. **B:** Contralateral projection of the PV1 neurons. EGFP-positive axons course in the supraoptic decussation and green terminals (white arrows) are close to PV-positive PV1-neurons (red) of the opposite side. **B1,B2:** Original images from which the merged image B was generated. The white arrow in B1 indicates axons in the supraoptic decussation and the rectangle in B2 shows the boundaries of the merged image B. Injection 502/12. **C:** Some endings are visible in the ipsilateral lateral habenular nucleus (experiment 237/12). In experiments with inadvertent labeling of the medial globus pallidus, the density of terminals is much higher (inset, injection 238/12). **D:** Axons probably deriving from the PV1 in the ipsilateral region around the retroflex fascicle. The axons then converge medially and are visible as a compact bundle adjacent to the EW, some sections later (asterisks in E). **E:** Compact bundles of axons in the region of the EW (asterisks). The section is counterstained with an antibody to CART, a marker of the centrally projecting part of the EW nucleus (green neurons). Terminals are located slightly more laterally (white arrow). The vertical dashed line represents the midline. Injection 64/12. **F:** Terminals are sometimes present in the dorsal tegmental nucleus (dTG). Their number increases drastically when the lateral mamillary nucleus is inadvertently costained (inset, white arrow). Injection 238/11. For abbreviations, see list. A magenta–green version of this image is included as supplementary Figure 3. Scale bar = 0.2 mm in A,C,D,F; 50 µm in E; 30 µm in B.

globus pallidus, the subthalamic nucleus, or the lateral mammillary nucleus, as were scattered cells in the medial hypothalamus that send dendrites to the PV1 nucleus. The extent of this spread is summarized in Table 4. Control injections targeted to these diverse nuclei failed to label terminals in the ventrolateral part

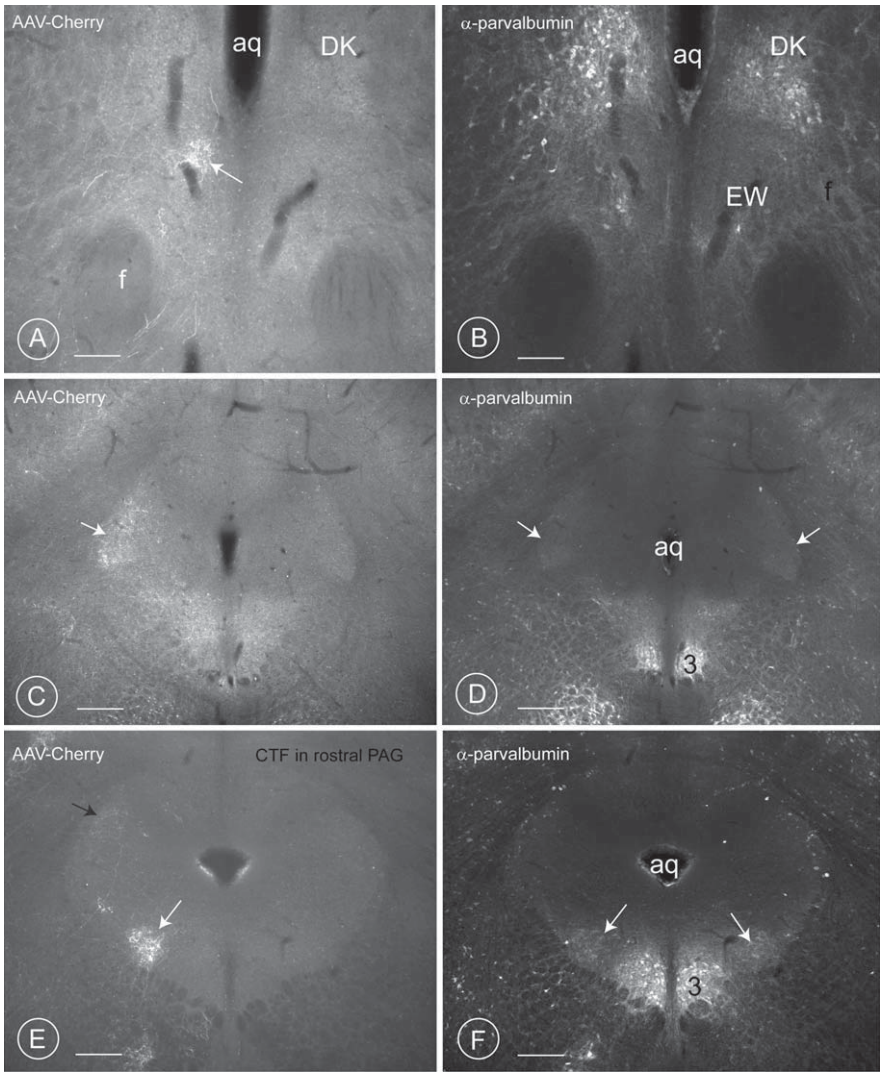

Figure 7. Distribution of terminal fields in the rostral PAG of mice. Three different levels of the mesencephalic PAG are reproduced, from the most rostral (A: Bregma −2.54), to the most caudal (F: Bregma −4.30). A, C, and E represent the terminal fields of the AAV–cherry-positive projections stemming from the PV1 nucleus. B, D, and F show the immunohistochemical revelation of the calcium-binding protein PV. **A,B:** The first terminal field of axons deriving from the PV1 nucleus (arrow in A) occurs at the level of the Edinger–Westphal nucleus (B), below the nucleus of Darkschewitz (DK, in A and B). **C,D:** The second terminal field of AAV–cherry-positive axons deriving from the PV1 nucleus is observed in the outer shell of the lateral portion of the PAG (white arrow in C; level −3.88 in Paxinos and Franklin [2001]), which coincides with a cloud of PV-positive endings (white arrows in D). Only scattered terminals from the PV1 are observed, indicating that most of the PV-positive endings in this region (D) have another source. The PV-positive neurons of the oculomotor nucleus (3) are visible ventromedially (D,F). Injection 64/12. **E,F:** The third, most prominent, terminal field is encountered ventrolateral to the aqueduct (white arrow in E) at the level of the oculomotor nucleus (3). This terminal field forms a longitudinally orientated cylinder (PV1-CTF), which spans approximately 450 μm in length (see also schematic drawing in Fig. 11). Compare this image with that of the retrograde injection in the rat PAG (Fig. 2A). Axons enter this fluffy aggregate of terminals from below, and some may come from lateral. The black arrow in E indicates scattered axons in the lateral PAG. Switching of the filter to visualize the PV immunostaining (F) reveals that the axons of the PV1 nucleus terminate in a territory rich in PV-positive endings, harboring only a few PV-positive neurons (bilateral white arrows in F) (injection 66/12, Table 4). For abbreviations, see list. Scale bar = 0.3 mm in A–F.

of the PAG (injections 189/11, 415/12, 416/1, 512/12 and 513/12; see Table 4).

Axons exited the rostral portion of the PV1 nucleus in the supraoptic commissure (Fig. 6B), its midregion in the medial forebrain bundle, and its distal portion in the dorsomedial direction (Fig. 5K). Fluorescent axons in the supraoptic commissure crossed the midline and ended in the contralateral region harboring the PV1 nucleus (Fig. 6B). Axons of neurons in the PV1 nucleus that ran in the medial forebrain bundle lateral to the mammillary bodies traced a wide path through the ventral tegmental region. At the level of the

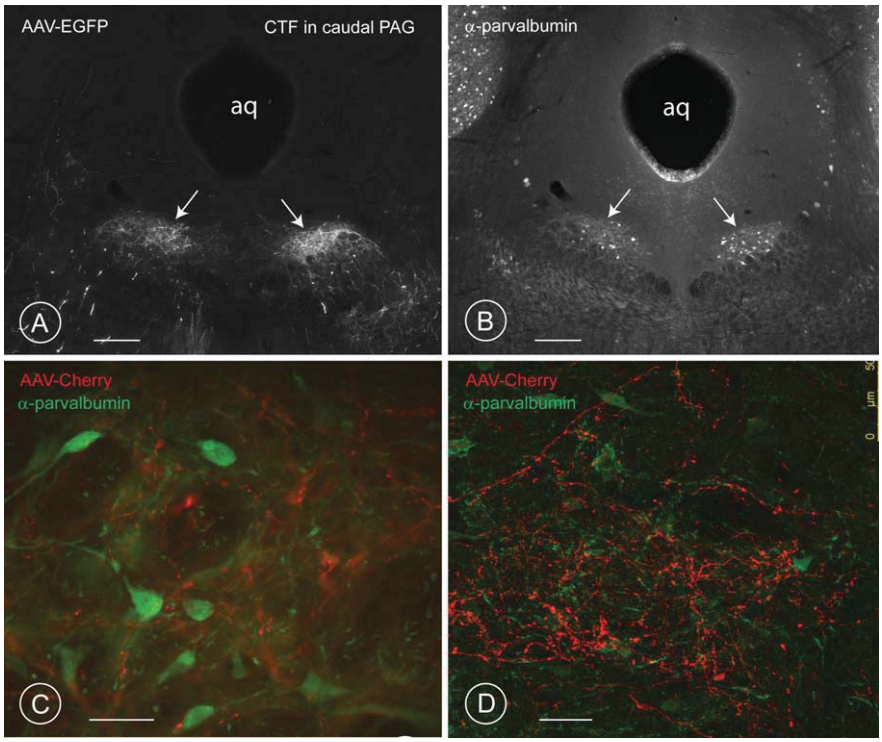

Figure 8. Distribution of terminal fields in the caudal PAG of mice. **A,B:** At the fourth and last level of the PAG (approximate level −4.6 in Paxinos and Franklin [2001]), the PV1-CTF flares out and becomes oval (white arrows in A), expands in the reticular formation, and impinges on a nucleus that is composed of PV-immunoreactive neurons (B). Notice the dense ipsilateral (right arrow) and the fainter contralateral PV1-CTF (left arrow). We have named this uncharted nucleus the PV2 nucleus (injection 503-12, bilaterally in the PV1 with the AAV2/9.CAG.FLEX.EGFP.WPRE.bGH constructs). **C,D**: At higher magnification, the density of terminals in the ventrolateral cylinder of terminals can be better appreciated (injection 237/11). The intimate relationship between the endings from the PV1 nucleus (red) and the PV-positive neurons in the PV2 nucleus (green) suggests possible synaptic contacts. **C:** Image taken with the fluorescence microscope (injection 237/11). **D:** Stack of laser scanning confocal images to visualize a similar level to C in injection 218/11. For abbreviations, see list. A magenta–green version of this image is included as supplementary Figure 4. Scale bar = 0.3 mm in A,B; 20 μm in C,D.

interpeduncular nucleus, the fibers curved dorsally along the midline, converged around the fasciculus retroflexus (Fig. 6D), and were then concentrated in the region of the Edinger–Westphal nucleus (Fig. 7A). A second component ran in the descending medial forebrain bundle into the ventromedial tegmentum at the level of the red nucleus, arched dorsolaterally, and then entered the ventrolateral part of the PAG at the level of the oculomotor nuclei (Fig. 7C–E).

In the PAG, the axons stemming from the PV1 nucleus terminated mainly ipsilaterally, ventrolateral to the aqueduct on the edge of the PAG in the Su3 region (Paxinos and Franklin, 2001; Paxinos and Watson, 2009; Van Bockstaele et al., 1989) and more sparsely in the lateral region (Figs. 7C,D and E,F, 9A–H). The dense cloud of terminals ventrolateral to the aqueduct formed a cylindrical column of terminal fields (PV1-CTF) (Figs. 7E, 9A–D,G,H), whereas the lateral one was crescentic and contained scattered terminals (Figs. 7C, 9).

The (PV1-CTF) was detectable first at level Bregma −3.88 mm in the atlas of Paxinos and Franklin (2001) and continued until level Bregma −4.30 mm (rostral portion, Figs. 7E,F, 9A–D and 11). After an interruption of approximately 150–200 μm (Figs. 2C, 9F, 11), the PV1-CTF continued from −4.56 to 4.84 mm (caudal portion, Figs. 8A–D, 9F–H), thus spanning a total length of approximately 1 mm (see details in Table 4, specimens 64–66/12). The contralateral side also exhibited a similar column of lower terminal density (left in Fig. 8A). The diameter of the PV1-CTF in the rostral part was of approximately 0.2 mm (Figs. 7E, 9A–D), and the oval PV1-CTF in the caudal part was 0.4 × 0.2 mm (Figs. 8A,B, 9G,H).

The terminals in the lateral quadrant first appeared approximately at level Bregma −3.4 mm and continued until level −4.7 mm in the atlas of Paxinos and Franklin (2001). Both the PV1-CTF ventrolateral of the aqueduct and the lateral quadrant, were discernible as PV-rich areas in sections that had been immunohistochemically stained for PV (Fig. 7D, F). Qualitatively, the density of terminals in the PV1-CTF seemed to correlate with the number of virus-infected cell bodies in the PV1 nucleus

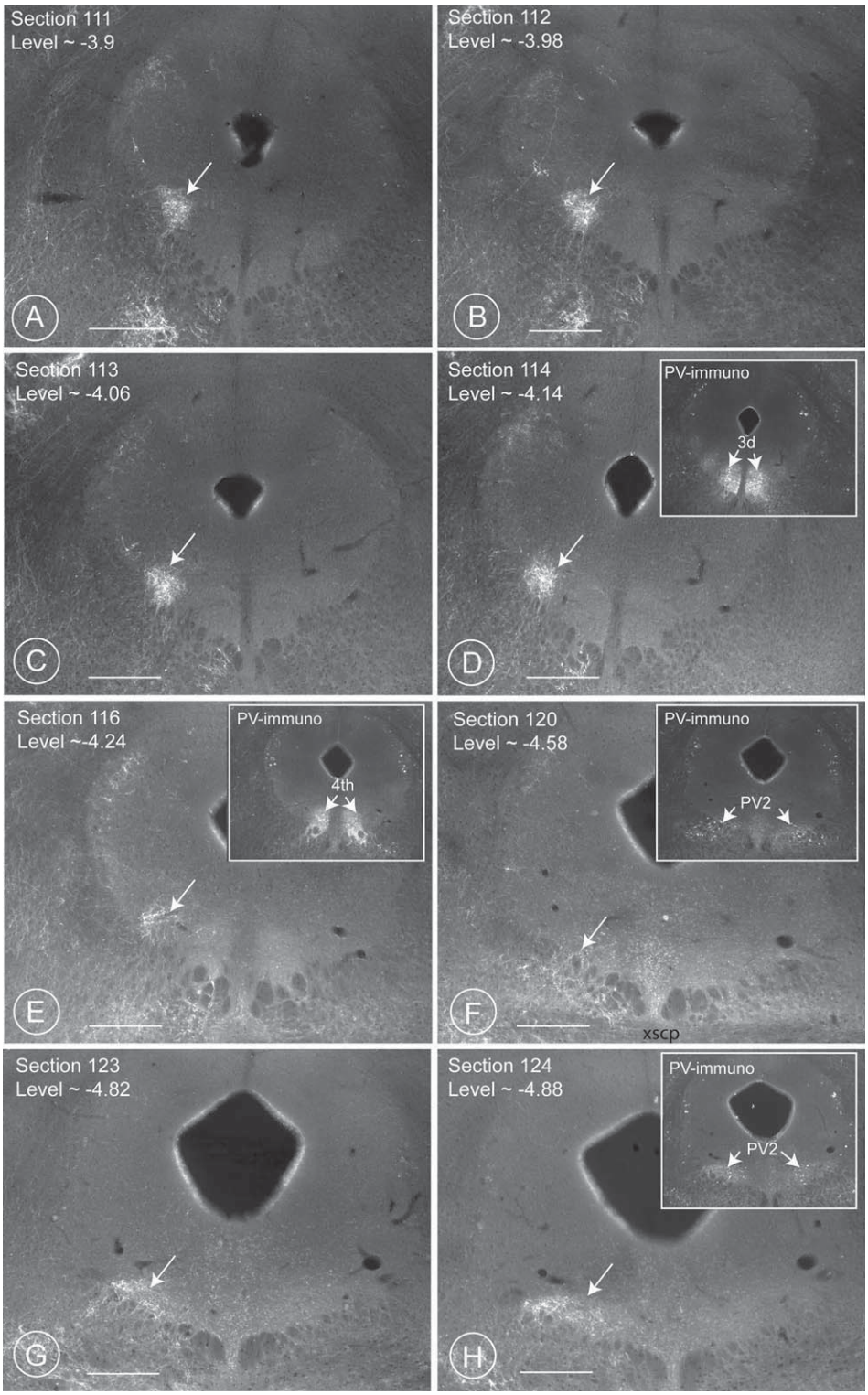

Figure 9. The cylindrical column of terminal fields (PV1-CTF) ventrolateral to the aqueduct. Images of eight consecutive sections cut through the periaqueductal gray region of brain 64/12. The dense and roundish terminal field ventrolateral to the aqueduct is highlighted by a white arrow and is clearly visible from levels 3.9 to 4.14 (A–D). It vanishes at level 4.24 (E) between section 117 and 119 (Bregma −4.30–4.50), reappears as an oval-shaped terminal field in section 120, and can be followed for some more sections (Figs. F–H), until section 125–126 (not shown). The insets in D, E, F, and H show the corresponding immunostaining with PV antibodies. Note the presence of the oculomotor nucleus at level 4.24 (D). The terminal field is absent in a stretch of approximately 250 μm, encompassing the region where the nucleus of the 4th cranial nerve (N. trochlearis) is located (inset in E). The PV2-nucleus is visible in the insets F and H. Compare these figures with the three-dimensional reconstruction in the drawing of Figure 11 (mouse) and Figure 2C (rat). Scale bar = 0.4 mm in A–H.

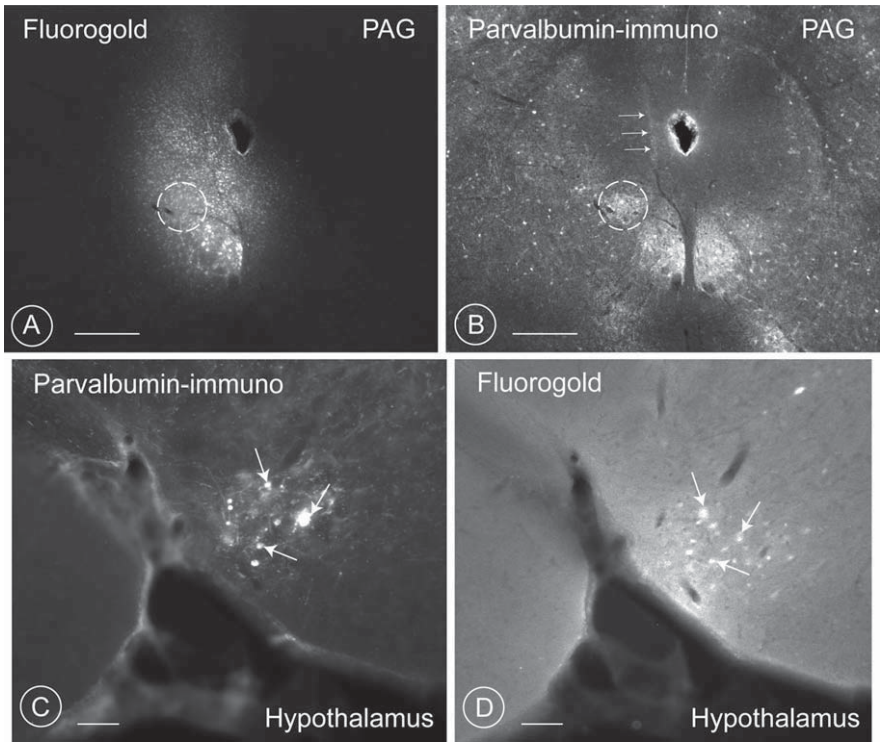

Figure 10. Retrograde labeling of neurons in the mouse PV1 nucleus after Fluoro-Gold injection at the level of the ventrolateral periaqueductal gray (PAG). **A,B:** Fluoro-Gold applied in the ventrolateral region of the PAG (A), including the region characterized by the presence of the PV1-CTF and a high concentration of PV-positive terminals (circles in A and B). Note the needle track in B (white horizontal arrows). **C,D:** At the level of the PV1 nucleus of the hypothalamus many neurons are filled with retrograde tracers (C), and three PV-positive neurons are indicated by arrows (D). Scale bar = 0.6 mm in A,B; 0.1 mm in C,D.

of different mice (Table 4). A precise quantification (e.g., by measuring fluorescence intensities with a confocal microscope) was not attempted. The terminal field ventrolateral to the aqueduct was sometimes traversed by large blood vessels (Fig. 4E,F).

At caudal levels between −4.56 and −4.84 mm (Paxinos and Franklin, 2001), the PV1-CTF impinged on an uncharted PV-positive population of neurons (Figs. 8A,B, 9F–H, 11). At this level the cylindrical column flares out and transcends the borders of the PAG to invade the adjoining reticular formation (Fig. 9F,G). The PV1-CTF is located medioventral as compared to the ventrolateral column of the PAG described by Bandler et al, 1994.

Injections of the tracer Fluoro-Gold in this same quadrant at various levels of the PAG resulted in the retrograde filling of PV-positive neurons in the PV1 nucleus of rats (Figs. 2C, 4A–H) and mice (Fig. 10). When injections were performed at level −7.10 (Fig. 2C, gap at the level of the trochlear nucleus) in the rat, no neurons of the PV1 nucleus could be retrogradely filled with Fluoro-Gold. In the mouse, neurons in the PV1 nucleus were retrogradely labeled only when the rostral or caudal PV1-CTF were hit (Fig. 10).

The outermost portion of the crescentic quadrant of the lateral PAG receives few terminals from the PV1 nucleus (Fig. 7D). In sections that were immunostained with antibodies against PV, this region is homogeneously labeled (Fig. 7E). We assume that the terminals originating from the PV1 nucleus constitute only a small proportion of the inputs to the lateral PAG. Embedded in the superficial, lateral portion of the caudal PAG are the large, PV-positive neurons of the mesencephalic trigeminal nucleus (Figs. 7F, 8B), which do not appear to be targeted by axons stemming from the PV1 nucleus. However, ultrastructural studies will be needed to confirm this impression.

The axon terminals coming from the PV1 nucleus were located more lateral than the cocaine- and amphetamine-regulated transcript (CART) neurons of the cortically projecting Edinger–Westphal subnucleus (Fig. 6E).

In some cases, in which large mCherry-labeled, PV-positive neurons were located more medially in the hypothalamus and in the lateral mammillary nucleus, terminals were identified in the dorsal tegmental nucleus (Fig. 6F). In two cases (189/11 and 218/11) the lateral mammillary nucleus was observed to contain

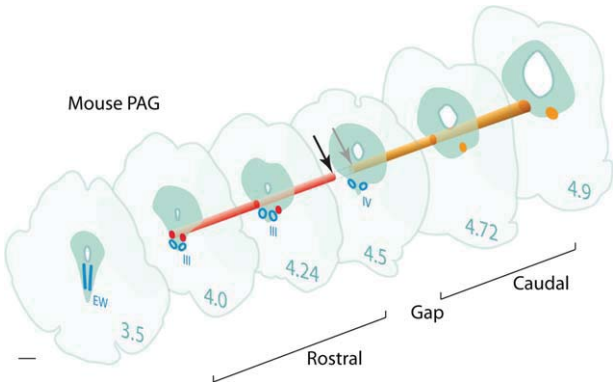

Figure 11. Three-dimensional reconstruction of the column of terminal fields (PV1-CTF). The mouse PAG is cut at six different rostrocaudal levels, revealing the approximate localization of the major terminal field (PV1-CTF) located ventrolateral to the aqueduct. The numbers indicate the different rostrocaudal levels in the atlas of Paxinos and Franklin (2001). The column of endings consists of two portions, a rostral (red) and a caudal (orange) field, between levels −4.0 mm and −4.9 mm, separated by a short gap (arrows) around −4.5 mm. For abbreviations, see list. Drawings modified from VanderHorst and Ulfhake (2006). Scale bar = 0.6 mm.

particularly large numbers of transduced neurons, and in those cases the dorsal tegmental nuclei were distinguished by the presence of intensely labeled terminal fields. The terminals probably do indeed derive from the lateral mammillary nucleus, via the mammillotegmental tract (Cruce, 1977; Hayakawa and Zyo, 1990).

In the tuberal hypothalamus, scattered large PV-positive neurons were seen with horizontal dendrites extending into the PV1 nucleus and were occasionally labeled with the viral construct. In control experiments that targeted only these neurons alone, no projection to the ventrolateral PAG was observed (case 416/12 and 513/12).

In two cases (189/11 and 64/12), which were distinguished by the presence of labeled neurons in the substantia nigra pars reticulata (SNr), inputs to the superior colliculus were particularly striking. The SNr is known to project to the superior colliculus (Cebrian et al., 2005); because the inputs to the latter were observed only when cells of the former region were targeted, they probably derive from it. In some specimens, a group of intensely labeled axons were seen that followed a vertical course near the fasciculus retroflexus (Fig. 6D) and then turned caudally in the ventral PAG. These axons appeared to stem mainly from the larger, most caudally located neurons of the PV1 nucleus, but terminals in the region of the retroflex fascicle could not be identified with certainty.

The projections of the reticular thalamic nucleus are confined to the thalamus, whereas those of the medial segment of the globus pallidus extend to the lateral habenular nucleus (Herkenham and Nauta, 1977), the subthalamic nucleus, and the substantia nigra (Carter and Fibiger, 1978). After an injection that left the medial segment of the pallidum unlabeled (237/11), only a few terminals (which possibly stemmed from the PV1 nucleus) were labeled in the lateral habenular nucleus. Hence, only a small proportion of the terminals in the latter structure originate from projections of the PV1 nucleus.

DISCUSSION

This hodological study has revealed that axons stemming from the elongated lateral hypothalamic PV1 nucleus terminate mainly ipsilaterally in a longitudinally oriented cylindrical field ventrolateral to the aqueduct. The injection of antero- and retrograde tracers into the lateral hypothalamus had hitherto disclosed numerous connections with rostral and caudal structures (Wolf and Sutin, 1966; Saper et al., 1979; Hosoya and Matsushita, 1980, 1981; Barone et al., 1981; Kita and Oomura, 1981, 1982; Berk and Finkelstein, 1982; Veening et al., 1987; Villalobos and Ferssiwi, 1987; Moga et al., 1990; Hurley et al., 1991). However, spatially more targeted injections have revealed that relatively few were related to the PV1 nucleus. Indeed, our findings indicate that the hypothalamic PV1 nucleus projects almost exclusively to the PAG. We observed no projections either to rostral targets, such as the septum and the amygdala, or to caudal ones, such as the parabrachial nuclei.

In some of the aforementioned tracer studies, the PV1 nucleus although not referred to as such was labeled, sometimes preferentially. For example, Berk and Finkelstein (1982) observed terminals in the lateral and ventrolateral PAG (case M15 in their Fig. 2I) after injection of tritiated amino acids into the distal portion of what we now recognize as the PV1 nucleus. In addition, after injection of PHA-L into the ventrolateral subarea of the lateral hypothalamus, which encompasses the PV1 nucleus, Veening et al. (1991) reported a similar distribution pattern of terminals ventrolateral to the aqueduct and to the dorsal raphe nucleus in rats (their Fig. 5B). Using tritiated leucin as an anterograde tracer in cats, Holstege (personal communication) recognized a similar pattern of projection from the lateral hypothalamus to the PAG.

In the present study, anterograde tracing from the PV1 nucleus in both rats and mice revealed terminal fields predominantly ventrolateral to the aqueduct on the edge of the PAG (Figs. 2C, 11; see also Paxinos and Franklin, 2001). In mice, the anterograde labeling

from the PV1 nucleus was more precise than in rats, thereby permitting the demonstration of a column of terminal fields (PV1-CTF) with a marked degree of topographical specificity in the PAG. This PV1-CTF is more medially located than the classical ventrolateral PAG-column reported in the literature (Bandler et al., 1991; Bandler and Shipley, 1994; Shipley et al., 1991), is of smaller caliber, and is axially restricted to the periphery of the PAG. The rostral target of the PV1 nucleus–derived PV1-CTF is localized along the lateral edge of the Su3 region (Paxinos and Franklin, 2001) in the rostral, *mes*encephalic part of the PAG. Spatially, the location of the PV1-CTF corresponds to that of a clearly demarcated PV-positive terminal field (Fig. 7E), thereby indicating that the immunoreactive endings stem mainly from the PV1 nucleus. Some faintly PV-positive neurons are also recognized in this superficial Su3 region. The connections of the Su3-containing region in rats have been studied by several groups of investigators (Maciewicz et al., 1975; Leichnetz et al., 1987; Giolli et al., 1988; Van Bockstaele et al., 1989, 1991) and have been implicated in oculomotor control (Vertes and Martin, 1988), in cortical activation, in REM sleep (Vertes, 1984), and, on the basis of the projection to the nucleus paragigantocellularis, also in autonomic control (Van Bockstaele et al., 1989). In cats, a high density of [^{3}H]quinuclidinyl benzilate (QNB) binding sites (pinpointing putative muscarinic receptors) has been revealed at a similar location in the PAG (Fig. 1 in Gundlach, 1991). A projection from the Su3 region to the nucleus gigantocellulairs pontis, which is implicated in eye movements, has also been detected (Torigoe et al., 1986).

The caudal portion of the PV1-CTF in the *met*encephalic part of the PAG abuts on a previously unrecognized cluster of PV-positive neurons (Figs. 8A,B, 9G–H) at rostrocaudal levels of −4.5 to −4.84 (Paxinos and Franklin, 2001). This area is referred to as the *substantia grisea centralis, pars ventralis* in the atlas of König and Klippel (1974), and is delineated but not named in Paxinos and Franklin (2001). In the publications that describe the parcellation of the PAG most comprehensively (Meller and Dennis, 1986; Clements et al., 1987; Ruiz-Torner et al., 2001), this region is not mentioned, and is only alluded to but rarely recognized in the literature as a whole. In cats, chemical stimulation of this region with D-L-homocysteic acid leads to a decrease in both blood pressure and vasoconstrictor tone of the renal vascular bed (Carrive, 1991; Harper et al., 1991), as well as quiescence and hyporeactivity (Depaulis et al., 1994). In the same species, lesioning of this region has been likewise shown to elicit a decrease in blood pressure as well as to prevent compensatory adjustments in arterial pressure during hemorrhaging (Ward and Darlington, 1987a,b). In the foreseeable future, tracer experiments involving the injection of Cre-dependent viral constructs into the distal PV1-CTF of PV-Cre mice (Hippenmeyer et al., 2005) will help to pinpoint the targets of this anonymous group of nerve cells, which we will henceforth refer to as the *PV2 nucleus*.

The short spatial interruption of the PV1-CTF that is revealed in rats and mice (see gap in Figs. 2C and 11) appears to be located at the level of the mesomere 2, a transverse, slender preisthmic territory interposed between the oculomotor and the trochlear nuclei (Puelles et al., 2012). The spatially coincidental localization of this gap in rats (Fig. 2C) and mice (Fig. 11) is striking.

The longitudinal orientation of the PV1-CTF accords with the hypothetical “functional longitudinal modules” of the PAG (Shipley et al., 1991) but corresponds to none of the other known columns. The PV1-CTF is located medial to the ventrolateral neuronal column as described by (Bandler et al,1991) and has a much smaller diameter. The PV2 nucleus occurs in its distal portion alone. Therefore the PV1-CTF, a putative, tiny “longitudinal module” is a chemoarchitectonically heterogeneous structure. This is consistent with the postulated functional heterogeneity of the rostrocaudal axis of other columns in the PAG (Bandler et al., 1991).

One issue that could not be unambiguously clarified in the present study relates to possible differences in the projection targets of the anteriorly located small neurons and the posteriorly located large ones in the PV1 nucleus (Meszar et al., 2012). In rats, injections of Fluoro-Gold into the dorsolateral tegmental nucleus (caudal portion of the PV1-CTF) and into the Su3 region (rostral portion of the PV1-CTF) revealed retrograde staining of both the small and the large cells in the PV1 nucleus (Fig. 4). In mice, injections of the same tracer into either the Su3 region (rostral PV1-CTF), or the PV2 nucleus (caudal PV1-CTF) of the PAG led to retrograde filling of the small as well as the large neurons, thereby ruling out any projection specificity.

Notwithstanding the very similar PV1-projection patterns ventrolateral to the aqueduct in the PAG of rats and mice (Figs. 2C, 11), some differences were observed between the two species. In rats, the PV1-CTF appears to run more caudally and to extend to the zone of the laterodorsal tegmental nucleus. In mice, more rostrally located structures, such as the Edinger–Westphal nucleus, received some terminals. These discrepancies could be attributable either to differences between the two species per se, or to differences in the methodological approach.

For example, species differences in traits that are influenced by the ventrolateral PAG regions close to the

PV1-CTF, e.g., vocalization, may be relevant. Depending on their affective state, rats vocalize at two different ultrasonic frequencies: 20 KHz and 50 KHz. The chirps produced at 20 KHz are implicated in situations that have a negative impact on the animals (Miczek et al., 1995), whereas the 50-KHz chirps are emitted in situations with a positive influence (Knutson et al., 1998). Although mice can draw on a rich repertoire of ultrasonic emissions, vocalization does not appear to be related to their affective state (Portfors, 2007).

In conclusion, the findings of the present study confirm the existence of an elongated PV1 nucleus within the lateral hypothalamus of rodents, and demonstrate that it sends out a major projection forming a column of terminal fields (PV1-CTF) located mainly ipsilateral, ventrolateral to the aqueduct on the edge of the PAG. This cylinder of terminal fields coincides with none of the classic longitudinal subdivisions of the PAG. Minor projections end in an identical location of the contralateral PAG, in the lateral habenular nucleus, the Edinger–Westphal nucleus, the reticular formation, and the laterodorsal tegmental nucleus. By virtue of its projections to a topographically restricted region ventrolateral to the aqueduct, the PV1 nucleus may presumably exert discrete functions. Testable functions of the PV1 nucleus include a possible involvement in analgesic, defensive, and sexual responses as well as in the autonomic adjustments that are indispensable for their successful expression. However, other functions unrelated to those classically attributed to the PAG are not to be excluded.

ACKNOWLEDGMENTS

The authors thank Profs. Tom Scammell (Harvard) and Joel Elmquist (now at the University of Texas Southwestern Medical Center, Dallas) for their continuous help and recommendations, and Dr. Rienk Tuinhof (deceased) for evaluating the double-labeled rat specimens. They are also grateful to Viktoria Szabolcsi and Alessandro Bilella for assistance with confocal microscope analysis and to Marlene Sanchez for technical help. Anwesha Bhattacharrya (MSc) was involved in the initial experiments with rats. The graphics for Figures 2 and 11 were prepared by Beat Brüsch (illustrateur@illustrateur.ch/www.embryology.ch). Several PhD students and postdoctoral assistants in the laboratory of C.S. performed the experiments that yielded the archival material, and the authors are grateful to Karen M. Hurley, Horst Herbert, and Margaret M. Moga for the permission to utilize these specimens. The adeno-associated viral constructs expressing cherry and red were received as a gift from Dr. K. Yonehara, who is a collaborator in the laboratory of Dr. Botond Roska (Friedrich Miescher Institute [FMI], Basle). Dr. Silvia Arber (FMI, Basle) kindly provided the PV-Cre mice. Some of the results described in this paper were presented at the European Neuroscience Meeting in Barcelona, 2012 (Babalian A, Clement L, Marti C, Celio MR. 2012. Projections of the PV nucleus of the lateral hypothalamus (PV1 nucleus) in the mouse. 8th FENS Abstracts vol. 6, 112.01).

CONFLICT OF INTEREST STATEMENT

The authors declare that they have no conflict of interest.

ROLE OF AUTHORS

All authors had full access to all the data in the study and take responsibility for the integrity of the data and the accuracy of the data analysis. MRC and CBS oversaw the project, evaluated and documented the results, and wrote the paper. AB made the stereotactic injections in mice, and SE and QHH those in rats. LC and CM prepared the sections and performed immunohistochemistry.

LITERATURE CITED

Bandler R, Shipley MT. 1994. Columnar organization in the midbrain periaqueductal gray: modules for emotional expression? Trends Neurosci 17:379–389.

Bandler R, Carrive P, Depaulis A. 1991. Introduction: emerging principles of organization of the midbrain periaqueductal gray matter. In: Depaulis A, Bandler R, editors. The midbrain periaqueductal gray matter. New York: Plenum. p 1–10.

Barone FC, Wayner MJ, Scharoun SL, Guevara-Aguilar R, Aguilar-Baturoni HU. 1981. Afferent connections to the lateral hypothalamus: a horseradish peroxidase study in the rat. Brain Res Bull 7:75–88.

Berk ML, Finkelstein JA. 1982. Efferent connections of the lateral hypothalamic area of the rat: an autoradiographic investigation. Brain Res Bull 8:511–526.

Bittencourt JC, Presse F, Arias C, Peto C, Vaughan J, Nahon JL, Vale W, Sawchenko PE. 1992. The melanin-concentrating hormone system of the rat brain: an immuno- and hybridization histochemical characterization. J Comp Neurol 319:218–245.

Carrive P. 1991. Functional organization of PAG neurons controlling regional vascular beds. In: Depaulis A, Bandler R, editors. The midbrain periaqueductal gray matter. New York: Plenum Press. p 67–100.

Carter DA, Fibiger HC. 1978. The projections of the entopeduncular nucleus and globus pallidus in rat as demonstrated by autoradiography and horseradish peroxidase histochemistry. J Comp Neurol 177:113–123.

Cebrian C, Parent A, Prensa L. 2005. Patterns of axonal branching of neurons of the substantia nigra pars reticulata and pars lateralis in the rat. J Comp Neurol 492:349–369.

Celio MR. 1990. Calbindin D-28k and parvalbumin in the rat nervous system. Neuroscience 35:375–475.

Chemelli RM, Willie JT, Sinton CM, Elmquist JK, Scammell T, Lee C, Richardson JA, Williams SC, Xiong Y, Kisanuki Y, Fitch TE, Nakazato M, Hammer RE, Saper CB, Yanagisawa

M. 1999. Narcolepsy in orexin knockout mice: molecular genetics of sleep regulation. Cell 98:437–451.
Chi CC, Flynn JP. 1971. Neural pathways associated with hypothalamically elicited attach behavior in cats. Science 171:703–706.
Clements JR, Madl JE, Johnson RL, Larson AA, Beitz AJ. 1987. Localization of glutamate, glutaminase, aspartate and aspartate aminotransferase in the rat midbrain periaqueductal gray. Exp Brain Res 67:594–602.
Cruce JA. 1977. An autoradiographic study of the descending connections of the mammillary nuclei of the rat. J Comp Neurol 176:631–644.
Depaulis A, Keay KA, Bandler R. 1994. Quiescence and hyporeactivity evoked by activation of cell bodies in the ventrolateral midbrain periaqueductal gray of the rat. Exp Brain Res 99:75–83.
Giolli RA, Torigoe Y, Blanks RH. 1988. Nonretinal projections to the medial terminal accessory optic nucleus in rabbit and rat: a retrograde and anterograde transport study. J Comp Neurol 269:73–86.
Girard F, Meszar Z, Marti C, Davis FP, Celio MR. 2011. Gene-expression profiles in the parvalbumin-immunoreactive (PV1) nucleus of the mouse lateral hypothalamus Eur J Neurosci 34:1934–1943.
Guillery RW. 1957. Degeneration in the hypothalamic connexions of the albino rat. J Anat 91:91–115.
Gundlach AL. 1991. Regional subdivisions in the midbrain periaqueductal gray of the cat revealed by in vitro receptor autoradiography. In: Depaulis A, Bandler R, editors. The midbrain periaqueductal gray matter. New York: Plenum Press. p 449–464.
Hahn JD, Swanson LW. 2010. Distinct patterns of neuronal inputs and outputs of the juxtaparaventricular and suprafornical regions of the lateral hypothalamic area in the male rat. Brain Res Rev 64:14–103.
Hahn JD, Swanson LW. 2012. Connections of the lateral hypothalamic area juxtadorsomedial region in the male rat. J Comp Neurol 520:1831–1890.
Harper RM, Ni H, Zhang J. 1991. Discharge relationship of periaqueductal gray neurons to cardiac and respiratory pattern during sleep and waking states. In: Depaulis A, Bandler R, editors. The midbrain periaqueductal gray matter. New York: Plenum Press. p 41–56.
Hayakawa T, Zyo K. 1990. Fine structure of the lateral mammillary projection to the dorsal tegmental nucleus of Gudden in the rat. J Comp Neurol 298:224–236.
Herbert H, Saper CB. 1992. Organization of medullary adrenergic and noradrenergic projections to the periaqueductal gray matter in the rat. J Comp Neurol 315:34–52.
Herbert H, Moga MM, Saper CB. 1990. Connections of the parabrachial nucleus with the nucleus of the solitary tract and the medullary reticular formation in the rat. J Comp Neurol 293:540–580.
Herkenham M, Nauta WJ. 1977. Afferent connections of the habenular nuclei in the rat. A horseradish peroxidase study, with a note on the fiber-of-passage problem. J Comp Neurol 173:123–146.
Hippenmeyer S, Vrieseling E, Sigrist M, Portmann T, Laengle C, Ladle DR, Arber S. 2005. A developmental switch in the response of DRG neurons to ETS transcription factor signaling. PLoS Biol 3:e159.
Hosoya Y, Matsushita M. 1980. Cells of origin of the descending afferents to the lateral hypothalamic area in the rat, studied with the horseradish peroxidase method. Neurosci Lett 18:231–236.
Hosoya Y, Matsushita M. 1981. Brainstem projections from the lateral hypothalamic area in the rat, as studied with autoradiography. Neurosci Lett 24:111–116.
Hurley KM, Herbert H, Moga MM, Saper CB. 1991. Efferent projections of the infralimbic cortex of the rat. J Comp Neurol 308:249–276.
Kirouac GJ, Parsons MP, Li S. 2006. Innervation of the paraventricular nucleus of the thalamus from cocaine- and amphetamine-regulated transcript (CART) containing neurons of the hypothalamus. J Comp Neurol 497:155–165.
Kita H, Oomura Y. 1981. Reciprocal connections between the lateral hypothalamus and the frontal complex in the rat: electrophysiological and anatomical observations. Brain Res 213:1–16.
Kita H, Oomura Y. 1982. An HRP study of the afferent connections to rat lateral hypothalamic region. Brain Res Bull 8:63–71.
Knutson B, Burgdorf J, Panksepp J. 1998. Anticipation of play elicits high-frequency ultrasonic vocalizations in young rats. J Comp Psychol 112:65–73.
König JFR, Klippel RA. 1974. The rat brain: a stereotaxic atlas of the forebrain and lower parts of the brain stem. New York: Robert E. Krieger.
Leichnetz GR, Hardy SG, Carruth MK. 1987. Frontal projections to the region of the oculomotor complex in the rat: a retrograde and anterograde HRP study. J Comp Neurol 263:387–399.
Maciewicz RJ, Kaneko CR, Highstein SM, Baker R. 1975. Morphophysiological identification of interneurons in the oculomotor nucleus that project to the abducens nucleus in the cat. Brain Res 96:60–65.
Meller ST, Dennis BJ. 1986. Afferent projections to the periaqueductal gray in the rabbit. Neuroscience 19:927–964.
Meszar Z, Girard F, Saper CB, Celio MR. 2012. The lateral hypothalamic parvalbumin-immunoreactive (PV1) nucleus in rodents. J Comp Neurol 520:798–815.
Miczek KA, Weerts EM, Vivian JA, Barros HM. 1995. Aggression, anxiety and vocalizations in animals: GABAA and 5-HT anxiolytics. Psychopharmacology (Berl) 121:38–56.
Moga MM, Herbert H, Hurley KM, Yasui Y, Gray TS, Saper CB. 1990. Organization of cortical, basal forebrain, and hypothalamic afferents to the parabrachial nucleus in the rat. J Comp Neurol 295:624–661.
Paxinos G, Franklin KBJ. 2001. The mouse brain in stereotaxic coordinates. San Diego: Academic Press.
Paxinos G, Watson C. 1999. The rat brain in stereotaxic coordinates. San Diego: Elsevier.
Paxinos G, Watson CW. 2009. The rat brain in stereotaxic coordinates. San Diego: Academic Press.
Peyron C, Tighe DK, van den Pol AN, de Lecea L, Heller HC, Sutcliffe JG, Kilduff TS. 1998. Neurons containing hypocretin (orexin) project to multiple neuronal systems. J Neurosci 18:9996–10015.
Portfors CV. 2007. Types and functions of ultrasonic vocalizations in laboratory rats and mice. J Am Assoc Lab Anim Sci 46:28–34.
Puelles E, Martinez de la Torre M, Watson CW, Puelles L. 2012. Midbrain. In: Watson CW, Puelles L, editors. The mouse nervous system. Amsterdam: Elsevier. p 337–359.
Reeber SL, Sillitoe RV. 2011. Patterned expression of a cocaine- and amphetamine-regulated transcript peptide reveals complex circuit topography in the rodent cerebellar cortex. J Comp Neurol 519:1781–1796.
Ruiz-Torner A, Olucha-Bordonau F, Valverde-Navarro AA, Martinez-Soriano F. 2001. The chemical architecture of the rat's periaqueductal gray based on acetylcholinesterase histochemistry: a quantitative and qualitative study. J Chem Neuroanat 21:295–312.
Saper CB, Loewy AD, Swanson LW, Cowan WM. 1976. Direct hypothalamo-autonomic connections. Brain Res 117:305–312.

Saper CB, Swanson LW, Cowan WM. 1979. An autoradiographic study of the efferent connections of the lateral hypothalamic area in the rat. J Comp Neurol 183:689–706.

Schwaller B, Dick J, Dhoot G, Carroll S, Vrbova G, Nicotera P, Pette D, Wyss A, Bluethmann H, Hunziker W, Celio MR. 1999. Prolonged contraction-relaxation cycle of fast-twitch muscles in parvalbumin knockout mice. Am J Physiol 276:C395–403.

Shipley MT, Ennis M, Rizvi TA, Behbehani MM. 1991. Topographical specificity of forebrain inputs to the midbrain peraqueductal gray: evidence for discrete longitudinally organized columns. In: Depaulis A, Bandler R, editors. The midbrain periaqueductal gray matter. New York: Plenum Press.

Swanson LW. 2004. Brain maps: structure of the rat brain. Amsterdam: Elsevier.

Torigoe Y, Blanks RH, Precht W. 1986. Anatomical studies on the nucleus reticularis tegmenti pontis in the pigmented rat. II. Subcortical afferents demonstrated by the retrograde transport of horseradish peroxidase. J Comp Neurol 243:88–105.

Van Bockstaele EJ, Pieribone VA, Aston-Jones G. 1989. Diverse afferents converge on the nucleus paragigantocellularis in the rat ventrolateral medulla: retrograde and anterograde tracing studies. J Comp Neurol 290:561–584.

Van Bockstaele EJ, Aston-Jones G, Pieribone VA, Ennis M, Shipley MT. 1991. Subregions of the periaqueductal gray topographically innervate the rostral ventral medulla in the rat. J Comp Neurol 309:305–327.

VanderHorst VG, Ulfhake B. 2006. The organization of the brainstem and spinal cord of the mouse: relationships between monoaminergic, cholinergic, and spinal projection systems. J Chem Neuroanat 31:2–36.

Veening G, Buma P, Ter Horst GJ, Roeling TAP, Luiten PGM, Nieuwenhuys R. 1991. Hypothalamic projections to the PAG in the rat: topographical, immuno–electronmicroscopical and functional aspects. In: Depaulis A, Bandler R, editors. The midbrain periaqueductal gray matter. New York: Plenum Press.

Veening JG, Lie ST, Geeraedts LMG, Nieuwenhuys R. 1987. A topographial analysis of the origin of some efferent projections from the lateral hypothalamus area in the rat. Neuroscience 22:537–551.

Vertes RP. 1984. Brainstem control of the events of REM sleep. Prog Neurobiol 22:241–288.

Vertes RP, Martin GF. 1988. Autoradiographic analysis of ascending projections from the pontine and mesencephalic reticular formation and the median raphe nucleus in the rat. J Comp Neurol 275:511–541.

Villalobos J, Ferssiwi A. 1987. The differential descending projections from the anterior, central and posterior regions of the lateral hypothalamic area: an autoradiographic study. Neurosci Lett 81:95–99.

Ward DG, Darlington DN. 1987a. A blood pressure lowering effect of lesions of the caudal periaqueductal gray: relationship to basal pressure. Brain Res 423:373–377.

Ward DG, Darlington DN. 1987b. Lesions of the caudal periaqueductal gray prevent compensation of arterial pressure during hemorrhage. Brain Res 407:369–375.

Wolf G, Sutin J. 1966. Fiber degeneration after lateral hypothalamic lesions in the rat. J Comp Neurol 127:137–156.

Yonehara K, Balint K, Noda M, Nagel G, Bamberg E, Roska B. 2011. Spatially asymmetric reorganization of inhibition establishes a motion-sensitive circuit. Nature 469:407–410.